Available online at www.sciencedirect.com
SCIENCE DIRECT®
Comput. Methods Appl. Mech. Engrg. 194 (2005) 1479–1512
Computer methods in applied mechanics and engineering
www.elsevier.com/locate/cma

# Finite element response sensitivity analysis: a comparison between force-based and displacement-based frame element models

M. Barbato, J.P. Conte *

*Department of Structural Engineering, University of California at San Diego, 9500 Gilman Drive, La Jolla, CA 92093-0085, United States*

Received 24 October 2003; received in revised form 26 April 2004; accepted 26 April 2004

**Abstract**

This paper focuses on a comparison between displacement-based and force-based elements for static and dynamic response sensitivity analysis of frame type structures. Previous research has shown that force-based frame elements are superior to classical displacement-based elements enabling, at no significant additional computational costs, a drastic reduction in the number of elements required for a given level of accuracy in the simulated response. The present work shows that this advantage of force-based over displacement-based elements is even more conspicuous in the context of gradient-based optimization methods, which are used in several structural engineering sub-fields (e.g., structural optimization, structural reliability analysis, finite element model updating) and which require accurate and efficient computation of structural response and response sensitivities to material and loading parameters. The two methodologies for displacement-based and force-based element sensitivity computations are compared. Three application examples are presented to illustrate the conclusions. Material-only non-linearity is considered. Significant benefits are found in using force-based frame element models for both response and response sensitivity analysis in terms of trade-off between accuracy and computational cost.


*Keywords:* Plasticity-based finite element models; Response sensitivity analysis; Force-based frame elements

* Corresponding author.
*E-mail address:* jpconte@ucsd.edu (J.P. Conte).

0045-7825/$ - see front matter © 2004 Elsevier B.V. All rights reserved.
doi:10.1016/j.cma.2004.04.011

## 1. Introduction

In recent years, great advances in the non-linear analysis of frame structures were led by the development of force-based elements, which have been found superior to classical displacement-based elements in tracing material non-linearities such as those encountered in steel, reinforced concrete, and composite frame structures (see [12–15]). The state-of-the-art in computational simulation of frame structures subjected to static and dynamic loads is in the non-linear domain to capture the complex behavior of structural systems when approaching their failure range.

Maybe even more important than the simulated non-linear response of a frame structure is its sensitivity to various geometric, mechanical, and material properties defining the structure and to loading parameters. Significant research has been devoted to the general problem of design sensitivity analysis (see [1,2,16,17]). Consistent finite element response sensitivity analysis methods are already well established for displacement-based finite elements (see [4,6,10,18]).

More recently, a procedure for response sensitivity computation using force-based frame elements has been developed [5] by the authors. This new procedure allows the use of force-based frame elements as a powerful simulation tool in applications which require finite element response sensitivity analysis results. Finite element response sensitivities represent an essential ingredient for gradient-based optimization methods needed in structural reliability analysis, structural optimization, structural identification, and finite element model updating (see [7,10]).

This paper presents a careful comparison between the response sensitivity computation methodologies for force-based and displacement-based frame elements in the context of materially-non-linear-only analysis. Both material and discrete loading parameters are considered. Three application examples involving quasi-static and dynamic loadings illustrate the different features of the two formulations in terms of computational effort and accuracy. Consistent finite element response sensitivities are compared with analytical (exact) when available. Conclusions are drawn about the relative merits of the displacement-based and force-based approaches for finite element response sensitivity analysis.

## 2. Response sensitivity analysis at the structure level

The computation of finite element response sensitivities to material and loading parameters requires extension of the finite element algorithms for response computation only. Let $r(t)$ denote a generic scalar response quantity (displacement, acceleration, local or resultant stress, etc.). By definition, the sensitivity of $r(t)$ with respect to the material or loading parameter $\theta$ is expressed mathematically as the (absolute) partial derivative of $r(t)$ with respect to the variable evaluated at $\theta = \theta_0$, i.e., $\partial r(t)/\partial\theta|_{\theta=\theta_0}$ where $\theta_0$ denotes the nominal value taken by the sensitivity parameter $\theta$ for the finite element response analysis.

In the sequel, following the notation proposed by Kleiber [10], the scalar response quantity $r(\boldsymbol{\vartheta}) = r(\mathbf{f}(\boldsymbol{\vartheta}), \boldsymbol{\vartheta})$ depends on the parameter vector $\boldsymbol{\vartheta}$ (defined by $n$ time-independent sensitivity parameters, i.e., $\boldsymbol{\vartheta} = [\theta_1, \ldots, \theta_n]^{\mathrm{T}}$), both explicitly and implicitly through the vector function $\mathbf{f}(\boldsymbol{\vartheta})$. It is assumed that $\frac{\mathrm{d}r}{\mathrm{d}\boldsymbol{\vartheta}}$ denotes the sensitivity gradient or total derivative of $r$ with respect to $\boldsymbol{\vartheta}$, $\frac{\mathrm{d}r}{\mathrm{d}\theta_i}$ is the absolute partial derivative of the argument $r$ with respect to the scalar variable $\theta_i$, $i = 1, \ldots, n$, (i.e., the derivative of the quantity $r$ with respect to the parameter $\theta_i$ considering explicit and implicit dependencies), while $\frac{\partial r}{\partial \theta_i}|_{\mathbf{z}}$ is the partial derivative of $r$ with respect to parameter $\theta_i$ when the vector of variables $\mathbf{z}$ is kept constant/fixed. In the particular, but important case in which $\mathbf{z} = \mathbf{f}(\boldsymbol{\vartheta})$, the expression $\frac{\partial r}{\partial \theta_i}|_{\mathbf{z}}$ reduces to the partial derivative of $r$ considering only the explicit dependency of $r$ on parameter $\theta_i$. For $\boldsymbol{\vartheta} = \theta_1 = \theta$ (single sensitivity parameter case), the adopted notation reduces to the usual elementary calculus notation. The derivations in the sequel consider the case of a single (scalar) sensitivity parameter $\theta$ without loss of generality, due to the uncoupled nature of the sensitivity equations with respect to multiple sensitivity parameters.

It is assumed herein that the response of a frame type structure is computed using a general-purpose non-linear finite element analysis program based on the direct stiffness method, employing suitable numerical integration schemes at both the structure and the element level. At each time step, after convergence of the incremental-iterative response computation, the consistent response sensitivities are calculated. According to the direct differentiation method (DDM) (see [4–6]), this requires the exact differentiation of the finite element numerical scheme for the response computation (including the numerical integration scheme for the material constitutive laws) with respect to the sensitivity parameter $\theta$ in order to obtain the "exact" sensitivities of the computationally simulated system response [1]. The DDM consists in computing first the conditional derivatives of the element and material history/state variables, forming the right-hand-side (RHS) of the response sensitivity equation at the structure level, solving it for the nodal displacement response sensitivities and updating the unconditional derivatives of all the history/state variables. The response sensitivity computation algorithm affects the various hierarchical layers of finite element response calculation, namely: (a) the structure level, (b) the element level, (c) the section level, and (d) the material level.

After spatial discretization using the finite element method, the equations of motion of a materially non-linear-only structural system take the form of the following non-linear matrix differential equation:

$$\mathbf{M}(\theta)\ddot{\mathbf{u}}(t,\theta) + \mathbf{C}(\theta)\dot{\mathbf{u}}(t,\theta) + \mathbf{R}(\mathbf{u}(t,\theta),\theta) = \mathbf{F}(t,\theta), \tag{1}$$

where $t$ = time, $\theta$ = scalar sensitivity parameter (material or loading variable), $\mathbf{u}(t)$ = vector of nodal displacements, $\mathbf{M}$ = mass matrix, $\mathbf{C}$ = damping matrix, $\mathbf{R}(\mathbf{u},t)$ = history dependent internal (inelastic) resisting force vector, $\mathbf{F}(t)$ = applied dynamic load vector, and a superposed dot denotes one differentiation with respect to time.

We assume without loss of generality that the time continuous-spatially discrete equation of motion (1) is integrated numerically in time using the well-known Newmark-$\beta$ time-stepping method of structural dynamics [3], yielding the following non-linear matrix algebraic equation in the unknowns $\mathbf{u}_{n+1} = \mathbf{u}(t_{n+1})$:

$$\mathbf{\Psi}(\mathbf{u}_{n+1}) = \widetilde{\mathbf{F}}_{n+1} - \left[\frac{1}{\beta(\Delta t)^2}\mathbf{M}\mathbf{u}_{n+1} + \frac{\alpha}{\beta(\Delta t)}\mathbf{C}\mathbf{u}_{n+1} + \mathbf{R}(\mathbf{u}_{n+1})\right] = \mathbf{0}, \tag{2}$$

where

$$\begin{aligned}\widetilde{\mathbf{F}}_{n+1} = \mathbf{F}_{n+1} &+ \mathbf{M}\left[\frac{1}{\beta(\Delta t)^2}\mathbf{u}_n + \frac{1}{\beta(\Delta t)}\dot{\mathbf{u}}_n - \left(1-\frac{1}{2\beta}\right)\ddot{\mathbf{u}}_n\right] \\ &+ \mathbf{C}\left[\frac{\alpha}{\beta(\Delta t)}\mathbf{u}_n - \left(1-\frac{\alpha}{\beta}\right)\dot{\mathbf{u}}_n - (\Delta t)\left(1-\frac{\alpha}{2\beta}\right)\ddot{\mathbf{u}}_n\right],\end{aligned} \tag{3}$$

$\alpha$ and $\beta$ are parameters controlling the accuracy and stability of the numerical integration algorithm and $\Delta t$ is the time increment. Eq. (2) represents the set of non-linear algebraic equations for the unknown response quantities $\mathbf{u}_{n+1}$ that has to be solved at each time step $[t_n, t_{n+1}]$. In general, the subscript $(\ldots)_{n+1}$ indicates that the quantity to which it is attached is evaluated at discrete time $t_{n+1}$.

We assume that $\mathbf{u}_{n+1}$ is the converged solution (up to some iteration residuals satisfying a specified tolerance usually taken in the vicinity of the machine precision) for the current time step $[t_n, t_{n+1}]$. Then, we differentiate Eq. (2) with respect to $\theta$ using the chain rule, recognizing that $\mathbf{R}(\mathbf{u}_{n+1}) = \mathbf{R}(\mathbf{u}_{n+1}(\theta),\theta)$ (i.e., the structure inelastic resisting force vector depends on $\theta$ both implicitly, through $\mathbf{u}_{n+1}$ and explicitly), which yields the following response sensitivity equation at the structure level:

[1] The computationally simulated system response is itself an approximation of the exact but unknown system response. The exact system response would require the exact solution of the (time continuous–space continuous) governing non-linear partial differential equations for the physical model of the structure under consideration.

$$\left[\frac{1}{\beta(\Delta t)^2}\mathbf{M}+\frac{\alpha}{\beta(\Delta t)}\mathbf{C}+(\mathbf{K}_{\mathrm{T}}^{\mathrm{stat}})_{n+1}\right]\frac{\mathrm{d}\mathbf{u}_{n+1}}{\mathrm{d}\theta}=-\left(\frac{1}{\beta(\Delta t)^2}\frac{\mathrm{d}\mathbf{M}}{\mathrm{d}\theta}+\frac{\alpha}{\beta(\Delta t)}\frac{\mathrm{d}\mathbf{C}}{\mathrm{d}\theta}\right)\mathbf{u}_{n+1}-\left.\frac{\partial\mathbf{R}(\mathbf{u}_{n+1}(\theta),\theta)}{\partial\theta}\right|_{\mathbf{u}_{n+1}}+\frac{\mathrm{d}\widetilde{\mathbf{F}}_{n+1}}{\mathrm{d}\theta},\tag{4}$$

where

$$\begin{aligned}\frac{\mathrm{d}\widetilde{\mathbf{F}}_{n+1}}{\mathrm{d}\theta}&=\frac{\mathrm{d}\mathbf{F}_{n+1}}{\mathrm{d}\theta}+\frac{\mathrm{d}\mathbf{M}}{\mathrm{d}\theta}\left(\frac{1}{\beta(\Delta t)^2}\mathbf{u}_n+\frac{1}{\beta(\Delta t)}\dot{\mathbf{u}}_n-\left(1-\frac{1}{2\beta}\right)\ddot{\mathbf{u}}_n\right)\\&+\mathbf{M}\left[\frac{1}{\beta(\Delta t)^2}\frac{\mathrm{d}\mathbf{u}_n}{\mathrm{d}\theta}+\frac{1}{\beta(\Delta t)}\frac{\mathrm{d}\dot{\mathbf{u}}_n}{\mathrm{d}\theta}-\left(1-\frac{1}{2\beta}\right)\frac{\mathrm{d}\ddot{\mathbf{u}}_n}{\mathrm{d}\theta}\right]\\&+\frac{\mathrm{d}\mathbf{C}}{\mathrm{d}\theta}\left[\frac{\alpha}{\beta(\Delta t)}\mathbf{u}_n-\left(1-\frac{\alpha}{\beta}\right)\dot{\mathbf{u}}_n-(\Delta t)\left(1-\frac{\alpha}{2\beta}\right)\ddot{\mathbf{u}}_n\right]\\&+\mathbf{C}\left[\frac{\alpha}{\beta(\Delta t)}\frac{\mathrm{d}\mathbf{u}_n}{\mathrm{d}\theta}-\left(1-\frac{\alpha}{\beta}\right)\frac{\mathrm{d}\dot{\mathbf{u}}_n}{\mathrm{d}\theta}-(\Delta t)\left(1-\frac{\alpha}{2\beta}\right)\frac{\mathrm{d}\ddot{\mathbf{u}}_n}{\mathrm{d}\theta}\right].\end{aligned}\tag{5}$$

The term $(\mathbf{K}_{\mathrm{T}}^{\mathrm{stat}})_{n+1}$ in Eq. (4) denotes the static consistent tangent stiffness matrix of the structure at time $t_{n+1}$. The second term on the RHS of Eq. (4) represents the partial derivative of the internal resisting force vector, $\mathbf{R}(\mathbf{u}_{n+1})$, with respect to sensitivity parameter $\theta$ under the condition that the displacement vector $\mathbf{u}_{n+1}$ remains fixed, and is computed through direct stiffness assembly of the element resisting force derivatives as

$$\left.\frac{\partial\mathbf{R}(\mathbf{u}_{n+1}(\theta),\theta)}{\partial\theta}\right|_{\mathbf{u}_{n+1}}=\sum_{e=1}^{N_{\mathrm{el}}}\left((\mathbf{A}_{\mathrm{b}}^{(e)})^{\mathrm{T}}\cdot\boldsymbol{\Gamma}_{\mathrm{REZ}}^{(e)\mathrm{T}}\cdot\boldsymbol{\Gamma}_{\mathrm{ROT}}^{(e)\mathrm{T}}\cdot\boldsymbol{\Gamma}_{\mathrm{RBM}}^{(e)\mathrm{T}}\cdot\left.\frac{\partial\mathbf{Q}_{n+1}}{\partial\theta}\right|_{\mathbf{q}_{n+1}}\right).\tag{6}$$

In the above equation, $\mathbf{A}_{\mathrm{b}}^{(e)}$ is the Boolean localization matrix for element "$e$"; $\boldsymbol{\Gamma}_{\mathrm{REZ}}^{(e)}$, $\boldsymbol{\Gamma}_{\mathrm{ROT}}^{(e)}$, and $\boldsymbol{\Gamma}_{\mathrm{RBM}}^{(e)}$ are kinematic transformation matrices to account for rigid end zones (REZ), rotation from global to local reference system (ROT), and rigid body modes (RBM), respectively; $\mathbf{q}_{n+1}$ and $\mathbf{Q}_{n+1}$ denote the vectors of basic element deformations and forces, respectively; and $N_{\mathrm{el}}$ denotes the number of frame elements in the structural model [5].

The above formulation, derived explicitly for dynamic response sensitivity analysis, contains the quasi-static case as a particular case, obtained by simply equating to zero in Eqs. (2)–(5) all terms containing the mass and damping matrices as well as their derivatives with respect to the sensitivity parameter $\theta$.

## 3. Response sensitivity analysis at the element level

Within the direct stiffness assembly formulation at the global/structure level, at every time/load step, the element inherits from the structure level the element nodal displacements $\mathbf{p}$, which are transformed into the basic element deformations $\mathbf{q}$, and returns the nodal resisting force vector $\mathbf{P}=\boldsymbol{\Gamma}_{\mathrm{REZ}}^{\mathrm{T}}\cdot\boldsymbol{\Gamma}_{\mathrm{ROT}}^{\mathrm{T}}\cdot\boldsymbol{\Gamma}_{\mathrm{RBM}}^{\mathrm{T}}\cdot\mathbf{Q}$ and the element consistent tangent stiffness matrix in global coordinates. The element interacts with the section level (or integration point level) transforming the element nodal deformations $\mathbf{q}$ into section deformations $\mathbf{d}$ and computing the basic element resisting forces $\mathbf{Q}$ from the section forces $\mathbf{D}$, themselves obtained through the material constitutive integration scheme. In a displacement-based formulation, the relationship between element deformations and section deformations on one hand and between element forces and section forces on the other hand is straightforward. In contrast, in the force-based formulation, there is no simple direct relation between the section deformations $\mathbf{d}$ and the basic element deformations $\mathbf{q}$, and an iterative proce-

dure (although a non-iterative one can also be used [12]) is used to perform the element state determination [14]. This fact complicates the derivation of the sensitivities of force-based element response quantities as compared to the case of displacement-based elements [6]. While for displacement-based elements, the derivative of the section deformations-element deformations relation is straightforward, since the section deformations depend on the sensitivity parameter $\theta$ only implicitly through the element deformations $\mathbf{q}(\theta)$, i.e., $\mathbf{d} = \mathbf{d}(x, \mathbf{q}(\theta))$ where $x$ denotes the coordinate along the beam axis, for force-based elements, the section deformations are function of $\theta$ both explicitly and implicitly, i.e., $\mathbf{d} = \mathbf{d}(x, \mathbf{q}(\theta), \theta)$ [5].

### 3.1. Displacement-based element response sensitivity computation

In a displacement-based element, the relationships between element and section deformations on one hand, and between element and section forces on the other hand are given by

$$\mathbf{d}(x,\theta) = \mathbf{B}(x) \cdot \mathbf{q}(\theta) \quad \text{(compatibility in strong form)}, \tag{7}$$

$$\mathbf{Q}(\theta) = \int_0^L \mathbf{B}^{\mathrm{T}}(x) \cdot \mathbf{D}(x,\theta) \cdot \mathrm{d}x \quad \text{(equilibrium in weak form)}, \tag{8}$$

where $\mathbf{B}(x)$ is a transformation matrix between element deformations and section deformations, which is independent of the sensitivity parameter $\theta$.

After introducing the normalized coordinate $\xi$ (with $-1 \leqslant \xi \leqslant 1$) and performing numerical integration, Eqs. (7) and (8) become

$$\mathbf{d}(\xi_i,\theta) = \mathbf{B}(\xi_i) \cdot \mathbf{q}(\theta) \quad (i = 1, \ldots, n_{\mathrm{IP}}), \tag{9}$$

$$\mathbf{Q}(\theta) = \frac{L}{2} \cdot \sum_{i=1}^{n_{\mathrm{IP}}} \{\mathbf{B}^{\mathrm{T}}(\xi_i) \cdot \mathbf{D}(\xi_i,\theta) \cdot w_i\}, \tag{10}$$

where $\xi_i$ and $w_i$ denote the sampling points and their integration weights, respectively, while $n_{\mathrm{IP}}$ represents the number of integration points along the beam axis.

Differentiation of the above relations is straightforward and yields

$$\frac{\mathrm{d}\mathbf{d}(\xi_i,\theta)}{\mathrm{d}\theta} = \mathbf{B}(\xi_i) \cdot \frac{\mathrm{d}\mathbf{q}(\theta)}{\mathrm{d}\theta} \quad (i = 1, \ldots, n_{\mathrm{IP}}), \tag{11}$$

$$\frac{\mathrm{d}\mathbf{Q}(\theta)}{\mathrm{d}\theta} = \frac{L}{2} \cdot \sum_{i=1}^{n_{\mathrm{IP}}} \left\{ \mathbf{B}^{\mathrm{T}}(\xi_i) \cdot \frac{\mathrm{d}\mathbf{D}(\xi_i,\theta)}{\mathrm{d}\theta} \cdot w_i \right\}. \tag{12}$$

Therefore, the element response sensitivity computation is easily accomplished using the following procedure (where the dependence of the various quantities on $\theta$ is not shown explicitly for the sake of brevity).

#### 3.1.1. Conditional derivatives (for $\boldsymbol{q}_{n+1}$ fixed)

(1) Set derivatives of the basic element deformations $\mathbf{q}_{n+1}$ to zero as1

$$\left.\frac{\partial \mathbf{q}_{n+1}}{\partial \theta}\right|_{\mathbf{q}_{n+1}} = \mathbf{0}. \tag{13}$$

It follows that:

$$\left.\frac{\partial \mathbf{d}_{n+1}(\xi_i)}{\partial \theta}\right|_{\mathbf{q}_{n+1}} = \mathbf{B}(\xi_i) \cdot \left.\frac{\partial \mathbf{q}_{n+1}}{\partial \theta}\right|_{\mathbf{q}_{n+1}} = \mathbf{0} \quad (i = 1, \ldots, n_{\mathrm{IP}}). \tag{14}$$

(2) From the constitutive law integration scheme (during loop over the element integration points for pre-response sensitivity calculations), compute $\left.\frac{\partial \mathbf{D}_{n+1}(\xi_i)}{\partial \theta}\right|_{\mathbf{q}_{n+1}}$ $(i = 1, \ldots, n_{\mathrm{IP}})$.

(3) Integrate the conditional derivatives of the sections forces over the element as

$$\left.\frac{\partial \mathbf{Q}_{n+1}}{\partial \theta}\right|_{\mathbf{q}_{n+1}} = \frac{L}{2} \cdot \sum_{i=1}^{n_{\mathrm{IP}}} \left\{ \mathbf{B}^{\mathrm{T}}(\xi_i) \cdot \left.\frac{\partial \mathbf{D}_{n+1}(\xi_i)}{\partial \theta}\right|_{\mathbf{q}_{n+1}} \cdot w_i \right\}. \tag{15}$$

(4) Form the RHS of the response sensitivity equation at the structure level, Eq. (4), through direct stiffness assembly.

(5) Solve Eq. (4) for the nodal response sensitivities, $\frac{\mathrm{d}\mathbf{u}_{n+1}}{\mathrm{d}\theta}$.

### 3.1.2. Unconditional derivatives

(1) Compute unconditional derivatives $\frac{\mathrm{d}\mathbf{q}_{n+1}}{\mathrm{d}\theta}$ from the solution of the response sensitivity equation at the structure level, Eq. (4), as

$$\frac{\mathrm{d}\mathbf{q}_{n+1}}{\mathrm{d}\theta} = \boldsymbol{\Gamma}^{(e)}_{\mathrm{RBM}} \cdot \boldsymbol{\Gamma}^{(e)}_{\mathrm{ROT}} \cdot \boldsymbol{\Gamma}^{(e)}_{\mathrm{REZ}} \cdot \frac{\mathrm{d}\mathbf{p}_{n+1}}{\mathrm{d}\theta} = \boldsymbol{\Gamma}^{(e)}_{\mathrm{RBM}} \cdot \boldsymbol{\Gamma}^{(e)}_{\mathrm{ROT}} \cdot \boldsymbol{\Gamma}^{(e)}_{\mathrm{REZ}} \cdot \mathbf{A}^{(e)}_{\mathrm{b}} \frac{\mathrm{d}\mathbf{u}_{n+1}}{\mathrm{d}\theta} \quad (e = 1, \ldots, N_{\mathrm{el}}). \tag{16}$$

The section deformation sensitivities are given by

$$\frac{\mathrm{d}\mathbf{d}_{n+1}(\xi_i)}{\mathrm{d}\theta} = \mathbf{B}(\xi_i) \cdot \frac{\mathrm{d}\mathbf{q}_{n+1}}{\mathrm{d}\theta} \quad (i = 1, \ldots, n_{\mathrm{IP}}). \tag{17}$$

(2) From the constitutive law integration scheme, compute and save the unconditional derivatives of the material and section history/state variables $\frac{\mathrm{d}\mathbf{r}_{n+1}(\xi_i)}{\mathrm{d}\theta}$ and compute $\frac{\mathrm{d}\mathbf{D}(\xi_i)}{\mathrm{d}\theta}$.

(3) Integrate the derivatives of the section forces over the element to obtain

$$\frac{\mathrm{d}\mathbf{Q}}{\mathrm{d}\theta} = \frac{L}{2} \cdot \sum_{i=1}^{n_{\mathrm{IP}}} \left\{ \mathbf{B}^{\mathrm{T}}(\xi_i) \cdot \frac{\mathrm{d}\mathbf{D}(\xi_i)}{\mathrm{d}\theta} \cdot w_i \right\} \tag{18}$$

## 3.2. Force-based element response sensitivity computation

In the most general case, the dependence of section deformations, $\mathbf{d}$, and section forces, $\mathbf{D}$, on the element deformations, $\mathbf{q}$, and sensitivity parameter, $\theta$, can be expressed as

$$\mathbf{d}(x, \theta) = \mathbf{d}(x, \mathbf{q}(\theta), \theta), \tag{19}$$

$$\mathbf{D}(x, \theta) = \mathbf{D}(\mathbf{d}(x, \mathbf{q}(\theta), \theta), \theta), \tag{20}$$

Using the chain rule of differentiation and referring to the normalized coordinate $\xi$, we determine the sensitivity of $\mathbf{d}$ and $\mathbf{D}$ to $\theta$ as

$$\frac{\mathrm{d}\mathbf{d}(\xi_i, \theta)}{\mathrm{d}\theta} = \left.\frac{\partial \mathbf{d}}{\partial \mathbf{q}}\right|_{\theta} \cdot \frac{\mathrm{d}\mathbf{q}(\theta)}{\mathrm{d}\theta} + \left.\frac{\partial \mathbf{d}}{\partial \theta}\right|_{\mathbf{q}} = \mathbf{B}(\xi_i, \theta) \cdot \frac{\mathrm{d}\mathbf{q}(\theta)}{\mathrm{d}\theta} + \left.\frac{\partial \mathbf{d}}{\partial \theta}\right|_{\mathbf{q}}, \tag{21}$$

$$\frac{\mathrm{d}\mathbf{D}(\xi_i,\theta)}{\mathrm{d}\theta} = \mathbf{k}_\mathrm{s}(\xi_i,\theta)\cdot\frac{\mathrm{d}\mathbf{d}(\xi_i,\theta)}{\mathrm{d}\theta} + \left.\frac{\partial\mathbf{D}}{\partial\theta}\right|_\mathbf{d} = \mathbf{k}_\mathrm{s}(\xi_i,\theta)\cdot\left[\mathbf{B}(\xi_i,\theta)\cdot\frac{\mathrm{d}\mathbf{q}(\theta)}{\mathrm{d}\theta} + \left.\frac{\partial\mathbf{d}}{\partial\theta}\right|_\mathbf{q}\right] + \left.\frac{\partial\mathbf{D}}{\partial\theta}\right|_\mathbf{d}, \tag{22}$$

where

$$\mathbf{B}(\xi_i,\theta) = \left.\frac{\partial\mathbf{d}}{\partial\mathbf{q}}\right|_\theta = \left.\frac{\partial\mathbf{d}}{\partial\mathbf{D}}\right|_\theta\cdot\left.\frac{\partial\mathbf{D}}{\partial\mathbf{Q}}\right|_\theta\cdot\left.\frac{\partial\mathbf{Q}}{\partial\mathbf{q}}\right|_\theta = \mathbf{f}_\mathrm{s}(\xi_i,\theta)\cdot\mathbf{b}(\xi_i)\cdot\mathbf{k}_\mathrm{T}^{(e)}(\theta), \tag{23}$$

$$\mathbf{k}_\mathrm{s}(\xi_i,\theta) = \left.\frac{\partial\mathbf{D}}{\partial\mathbf{d}}\right|_\theta = [\mathbf{f}_\mathrm{s}(\xi_i,\theta)]^{-1}. \tag{24}$$

In the above equations, $\mathbf{k}_\mathrm{s}$ and $\mathbf{f}_\mathrm{s}$ denote the section tangent stiffness and flexibility matrices, respectively, and $\mathbf{k}_\mathrm{T}$ is the element tangent stiffness matrix. Differentiating the equilibrium equations in strong form, $\mathbf{D}(\xi_i,\theta) = \mathbf{b}(\xi_i)\cdot\mathbf{Q}(\theta)$ (where $\mathbf{b}$ denotes the matrix of internal force interpolation functions), with respect to parameter $\theta$, assuming no element distributed loads, yields

$$\frac{\mathrm{d}\mathbf{D}(\xi_i,\theta)}{\mathrm{d}\theta} = \mathbf{b}(\xi_i)\cdot\frac{\mathrm{d}\mathbf{Q}(\theta)}{\mathrm{d}\theta}. \tag{25}$$

Compatibility between basic element deformations $\mathbf{q}$ and section deformations $\mathbf{d}$ (in weak form through the principle of virtual forces) is expressed, using the normalized coordinate $\xi$ and performing numerical integration, as

$$\mathbf{q}(\theta) = \frac{L}{2}\cdot\sum_{i=1}^{n_\mathrm{IP}}\{\mathbf{b}^\mathrm{T}(\xi_i)\cdot\mathbf{d}(\xi_i,\theta)\cdot w_i\}. \tag{26}$$

Differentiating the above relation with respect to parameter $\theta$, we obtain

$$\frac{\mathrm{d}\mathbf{q}(\theta)}{\mathrm{d}\theta} = \frac{L}{2}\cdot\sum_{i=1}^{n_\mathrm{IP}}\left\{\mathbf{b}^\mathrm{T}(\xi_i)\cdot\frac{\mathrm{d}\mathbf{d}(\xi_i,\theta)}{\mathrm{d}\theta}\cdot w_i\right\}. \tag{27}$$

It is necessary to derive both conditional (with $\mathbf{q}$ fixed) and unconditional derivatives of the basic element forces, $\mathbf{Q}$, and section deformations, $\mathbf{d}(\xi_i)$, and the unconditional derivatives of all other history/ state variables at the element, section, and material levels, respectively. For this purpose, we merge Eqs. (22) and (25) to obtain

$$\mathbf{k}_\mathrm{s}(\xi_i,\theta)\cdot\frac{\mathrm{d}\mathbf{d}(\xi_i,\theta)}{\mathrm{d}\theta} - \mathbf{b}(\xi_i)\cdot\frac{\mathrm{d}\mathbf{Q}(\theta)}{\mathrm{d}\theta} = -\left.\frac{\partial\mathbf{D}(\xi_i,\theta)}{\partial\theta}\right|_\mathbf{d}. \tag{28}$$

Equations for conditional derivatives of $\mathbf{Q}$ and $\mathbf{d}$ are obtained from Eqs. (27) and (28) by substituting $\frac{\mathrm{d}\mathbf{d}(\xi_i)}{\mathrm{d}\theta}$ with $\frac{\partial\mathbf{d}(\xi_i)}{\partial\theta}|_\mathbf{q}$ and $\frac{\mathrm{d}\mathbf{Q}}{\mathrm{d}\theta}$ with $\frac{\partial\mathbf{Q}}{\partial\theta}|_\mathbf{q}$ and setting $\frac{\partial\mathbf{q}}{\partial\theta}|_\mathbf{q} = \mathbf{0}$. Eqs. (27) and (28) provide a system of $(2n_{IP} + 3)$ equations with $(2n_\mathrm{IP} + 3)$ scalar unknowns. These scalar unknowns are $\frac{\partial\mathbf{d}(\xi_i)}{\partial\theta}|_\mathbf{q}$ or $\frac{\mathrm{d}\mathbf{d}(\xi_i)}{\mathrm{d}\theta}$ (two unknowns for each integration point), and $\frac{\partial\mathbf{Q}}{\partial\theta}|_\mathbf{q}$ or $\frac{\mathrm{d}\mathbf{Q}}{\mathrm{d}\theta}$ (three unknowns for each element), for conditional and unconditional derivatives, respectively. The conditional derivatives $\frac{\partial\mathbf{D}(\xi_i)}{\partial\theta}|_\mathbf{d}$ on the RHS of Eq. (28) can be obtained through conditional differentiation of the constitutive law integration scheme at the numerical integration point level. In Eqs. (21)–(28), $i = 1,\ldots,n_\mathrm{IP}$.

The response sensitivity computation scheme for force-based frame element is described in the sections below (where the dependence of the various quantities on $\theta$ is not shown explicitly).

### 3.2.1. Conditional derivatives (for $\mathbf{q}_{n+1}$ fixed)

(1) Set derivatives of the basic element deformations $\mathbf{q}_{n+1}$ and section deformations $\mathbf{d}_{n+1}(\xi_i)$ to zero (i.e., considering $\mathbf{q}_{n+1}$ and $\mathbf{d}_{n+1}(\xi_i)$, respectively, as fixed quantities) as

$$\left.\frac{\partial \mathbf{q}_{n+1}}{\partial \theta}\right|_{\mathbf{q}_{n+1}} = \mathbf{0}, \tag{29}$$

$$\left.\frac{\partial \mathbf{d}_{n+1}(\xi_i)}{\partial \theta}\right|_{\mathbf{d}_{n+1}} = \mathbf{0} \quad (i = 1, \ldots, n_{\mathrm{IP}}), \tag{30}$$

(2) From the constitutive law integration scheme (during loop over the element integration points for pre-response sensitivity calculations), compute $\frac{\partial \mathbf{D}_{n+1}(\xi_i)}{\partial \theta}|_{\mathbf{d}_{n+1}}$ and then set up the following linear system of $(2n_{\mathrm{IP}} + 3)$ equations (after looping over the integration points):

$$\begin{cases} \mathbf{k}_{\mathrm{s},n+1}(\xi_i) \cdot \left.\dfrac{\partial \mathbf{d}_{n+1}(\xi_i)}{\partial \theta}\right|_{\mathbf{q}_{n+1}} - \mathbf{b}(\xi_i) \cdot \left.\dfrac{\partial \mathbf{Q}_{n+1}}{\partial \theta}\right|_{\mathbf{q}_{n+1}} = -\left.\dfrac{\partial \mathbf{D}_{n+1}(\xi_i)}{\partial \theta}\right|_{\mathbf{d}_{n+1}} \\ \displaystyle\sum_{i=1}^{n_{\mathrm{IP}}} \left\{ \mathbf{b}^{\mathrm{T}}(\xi_i) \cdot \left.\frac{\partial \mathbf{d}_{n+1}(\xi_i)}{\partial \theta}\right|_{\mathbf{q}_{n+1}} \cdot w_i \right\} = \mathbf{0} \end{cases} \quad (i = 1, \ldots, n_{\mathrm{IP}}). \tag{31}$$

(3) Solve Eq. (31) for $\frac{\partial \mathbf{d}_{n+1}(\xi_i)}{\partial \theta}|_{\mathbf{q}_{n+1}}$ and $\frac{\partial \mathbf{Q}_{n+1}}{\partial \theta}|_{\mathbf{q}_{n+1}}$ $(i = 1, \ldots, n_{\mathrm{IP}})$.

(4) Form the RHS of the response sensitivity equation at the structure level, Eq. (4), through direct stiffness assembly.

(5) Solve Eq. (4) for the nodal response sensitivities, $\frac{\mathrm{d}\mathbf{u}_{n+1}}{\mathrm{d}\theta}$.

### 3.2.2. Unconditional derivatives

(1) Compute unconditional derivative $\frac{\mathrm{d}\mathbf{q}_{n+1}}{\mathrm{d}\theta}$ from the solution of the response sensitivity equation at the structure level, Eq. (4), as

$$\frac{\mathrm{d}\mathbf{q}_{n+1}}{\mathrm{d}\theta} = \boldsymbol{\Gamma}^{(e)}_{\mathrm{RBM}} \cdot \boldsymbol{\Gamma}^{(e)}_{\mathrm{ROT}} \cdot \boldsymbol{\Gamma}^{(e)}_{\mathrm{REZ}} \cdot \frac{\mathrm{d}\mathbf{p}_{n+1}}{\mathrm{d}\theta} = \boldsymbol{\Gamma}^{(e)}_{\mathrm{RBM}} \cdot \boldsymbol{\Gamma}^{(e)}_{\mathrm{ROT}} \cdot \boldsymbol{\Gamma}^{(e)}_{\mathrm{REZ}} \cdot \mathbf{A}^{(e)}_{\mathrm{b}} \frac{\mathrm{d}\mathbf{u}_{n+1}}{\mathrm{d}\theta} \quad (e = 1, \ldots, N_{\mathrm{el}}). \tag{32}$$

(2) Using the conditional derivatives $\frac{\partial \mathbf{D}_{n+1}(\xi_i)}{\partial \theta}|_{\mathbf{d}_{n+1}}$ computed during the pre-response sensitivity calculation phase, set up the following linear system of $(2n_{\mathrm{IP}} + 3)$ equations:

$$\begin{cases} \mathbf{k}_{\mathrm{s},n+1}(\xi_i) \cdot \dfrac{\mathrm{d}\mathbf{d}_{n+1}(\xi_i)}{\mathrm{d}\theta} - \mathbf{b}(\xi_i) \cdot \dfrac{\mathrm{d}\mathbf{Q}_{n+1}}{\mathrm{d}\theta} = -\left.\dfrac{\partial \mathbf{D}_{n+1}(\xi_i)}{\partial \theta}\right|_{\mathbf{d}_{n+1}} \\ \dfrac{L}{2} \cdot \displaystyle\sum_{i=1}^{n_{\mathrm{IP}}} \left\{ \mathbf{b}^{\mathrm{T}}(\xi_i) \cdot \frac{\mathrm{d}\mathbf{d}_{n+1}(\xi_i)}{\mathrm{d}\theta} \cdot w_i \right\} = \dfrac{\mathrm{d}\mathbf{q}_{n+1}}{\mathrm{d}\theta} \end{cases} \quad (i = 1, \ldots, n_{\mathrm{IP}}). \tag{33}$$

(3) Solve Eq. (33) for the unconditional derivatives $\frac{\mathrm{d}\mathbf{d}_{n+1}(\xi_i)}{\mathrm{d}\theta}(i = 1, \ldots, n_{\mathrm{IP}})$, and $\frac{\mathrm{d}\mathbf{Q}_{n+1}}{\mathrm{d}\theta}$.

(4) Perform a loop over the frame element integration points, entering with $\frac{\mathrm{d}\mathbf{d}_{n+1}(\xi_i)}{\mathrm{d}\theta}$ in the differentiated constitutive law integration scheme, compute and save the unconditional derivatives of the material and section history/state variables $\frac{dr_{n+1}(\xi_i)}{\mathrm{d}\theta}$. These unconditional derivatives are needed to compute the conditional derivatives required for response sensitivity computations at the next time step, $t_{n+2}$, namely, $\frac{\partial \mathbf{D}_{n+2}(\xi_i)}{\partial \theta}|_{\mathbf{d}_{n+2}}$, $\frac{\partial \mathbf{d}_{n+2}(\xi_i)}{\partial \theta}|_{\mathbf{q}_{n+2}}$ and $\frac{\partial \mathbf{Q}_{n+2}}{\partial \theta}|_{\mathbf{q}_{n+2}}$.

### 3.3. Implementation in a general-purpose non-linear finite element structural analysis program

For comparison purposes, the above formulations for response sensitivity analysis using displacement-based and force-based frame elements were implemented in a general-purpose finite element structural analysis program, namely FEDEASLab Release 2.2 [8]. FEDEASLab is a Matlab [11] toolbox suitable for linear and non-linear, static and dynamic structural analysis, which has the advantage to provide a general framework for physical parameterization of finite element models and response sensitivity computation [9].

One of the most important features of FEDEASLab is its strict modularity, that keeps separate the different hierarchical levels encountered in structural analysis (i.e., structure, element, section and material levels). Therefore, the use of displacement-based or force-based elements is not dependent or related to the use of any section model and/or material constitutive law (properly implemented with provisions for sensitivity analysis) and their present comparison is strictly and uniquely based on the different features of their response sensitivity computation scheme and performance in terms of accuracy and computational cost.

Flow-charts comparing the computer implementation of the response sensitivity analysis for the two different elements are presented in Figs. 1 and 2. It is worth noting two main differences between displacement-based [6] and force-based frame elements [5]: (a) in the displacement-based formulation, there is no need to solve a linear system of equations at the element level in order to obtain the conditional and unconditional derivatives of the nodal element forces $\frac{\partial \mathbf{Q}_{n+1}}{\partial \theta}\big|_{\mathbf{q}_{n+1}}$ and $\frac{\mathrm{d}\mathbf{Q}_{n+1}}{\mathrm{d}\theta}$, respectively; and (b) while for displacement-based elements, the condition $\mathbf{q}_{n+1}$ fixed is equivalent to the condition $\mathbf{d}_{n+1}(\xi_i)$ ($i = 1, 2, \ldots, n_{\mathrm{IP}}$) fixed, for force-based elements, it is necessary to compute the conditional derivatives of the history/state variables imposing $\mathbf{d}_{n+1}(\xi_i)$ fixed in order to obtain the conditional (for $\mathbf{q}_{n+1}$ fixed) and unconditional derivatives of the nodal element forces.

## 4. Application examples

### 4.1. Application example: cantilever beam with distributed plasticity

The first test structure considered in this paper is the cantilever $W21 \times 50$ steel I-beam 10 m in length shown in Fig. 3. The geometric properties of the beam cross-section are: $A = 9.484 \times 10^{-3}$ [m$^2$] (cross-section area) and $I = 4.096 \times 10^{-4}$ [m$^4$] (moment of inertia about strong axis) (see Fig. 3). Its initial yield moment is $M_{y0} = 384.2$ [kN m] and a 9.09% post-yield to initial flexural stiffness ratio is assumed. The axial behavior is assumed linear elastic, while the flexural behavior is modeled by a 1-D $J_2$ plasticity section constitutive law [6] with the following material parameters: Young's modulus $E = 2 \times 10^8$ [kPa], and isotropic and kinematic hardening moduli, $H_{\mathrm{iso}} = 0$ [kPa], $H_{\mathrm{kin}} = 2 \times 10^7$ [kPa], respectively. It is noteworthy that the 1-D $J_2$ plasticity for zero isotropic hardening reduces to the well known bi-linear constitutive model, with fixed post-yield stiffness (see Fig. 4(a)).

The simple load case of a quasi-static, monotonically increasing point load applied at the tip of the cantilever is considered, for which closed form solutions for both response and response sensitivities to material parameters can be easily derived through applying the principle of virtual forces (see Fig. 4). As response quantities, we considered the vertical tip displacement $U$ (global response quantity) and the cumulative plastic curvature $\overline{\chi}^{\mathrm{p}}$ at the fixed end of the cantilever (local response quantity). The analytical solutions for these two response quantities have been derived as

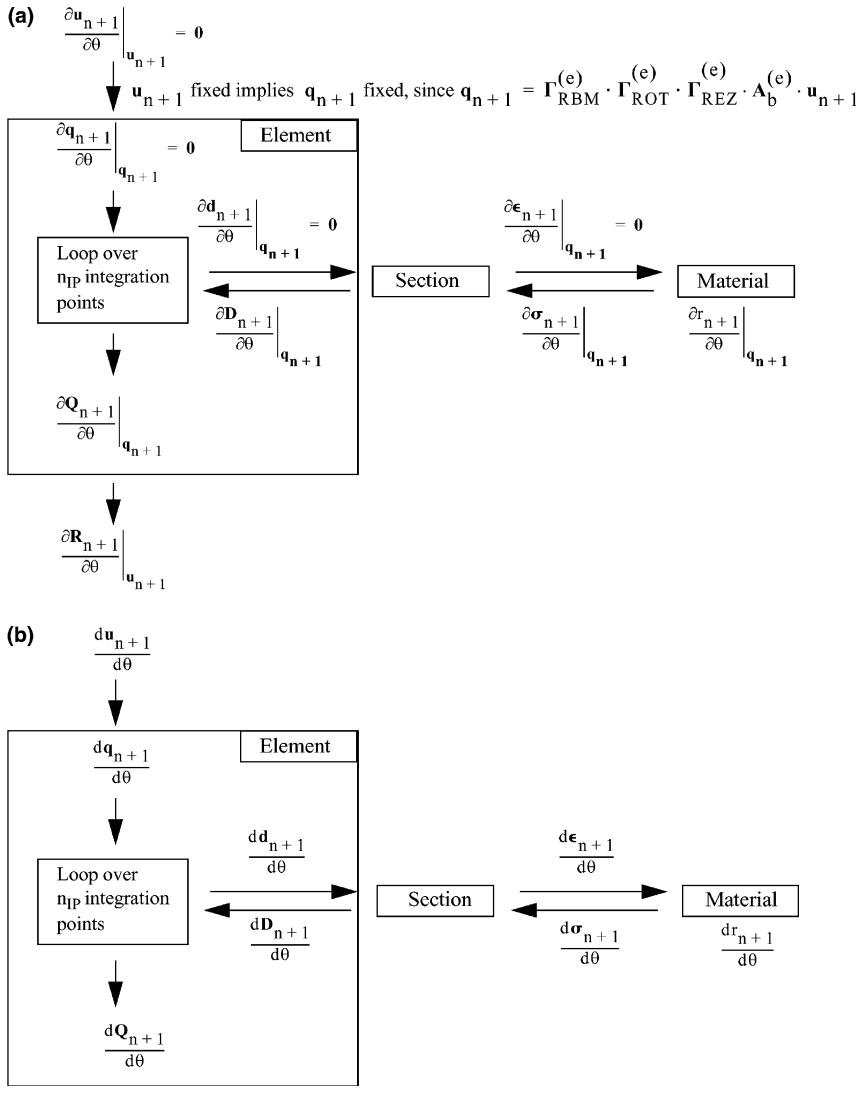


Fig. 1. Flow chart for the numerical computation of the response sensitivity with a displacement-based frame element: (a) conditional derivatives and (b) unconditional derivatives.

$$U = \begin{cases} \dfrac{PL^3}{3EI}; & \text{if } P \leqslant \dfrac{M_{y0}}{L}, \\ \dfrac{PL^3}{3EI}\left(\dfrac{H_{\text{kin}}+E}{H_{\text{kin}}}\right) - \dfrac{M_{y0}L^2}{2H_{\text{kin}}I} + \dfrac{M_{y0}^3}{6P^2H_{\text{kin}}I}; & \text{if } P > \dfrac{M_{y0}}{L}. \end{cases} \tag{34}$$

$$\overline{\chi}^{\text{p}} = \begin{cases} 0; & \text{if } P \leqslant \dfrac{M_{y0}}{L}, \\ \dfrac{PL - M_{y0}}{H_{\text{kin}}I}; & \text{if } P > \dfrac{M_{y0}}{L}. \end{cases} \tag{35}$$

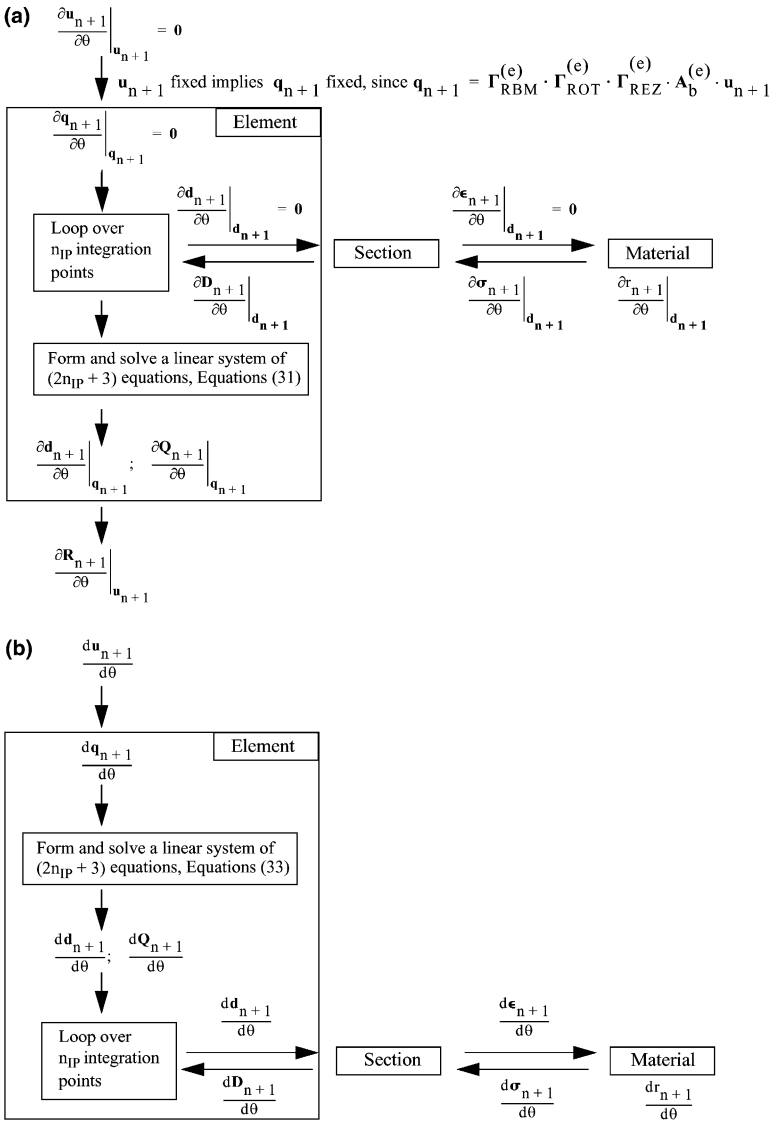


Fig. 2. Flow chart for the numerical computation of the response sensitivity with a force-based frame element: (a) conditional derivatives and (b) unconditional derivatives.

The vertical tip displacement sensitivities to material parameters $E$, $M_{y0}$, and $H_{kin}$ are given by

$$\frac{\mathrm{d}U}{\mathrm{d}E} = -\frac{PL^3}{3E^2I}, \tag{36}$$

$$\frac{\mathrm{d}U}{\mathrm{d}M_{y0}} = \begin{cases} 0; & \text{if } P \leqslant \dfrac{M_{y0}}{L}, \\ -\dfrac{1}{2H_{\mathrm{kin}}I}\left[L^2 - \left(\dfrac{M_{y0}}{P}\right)^2\right]; & \text{if } P > \dfrac{M_{y0}}{L}, \end{cases} \tag{37}$$

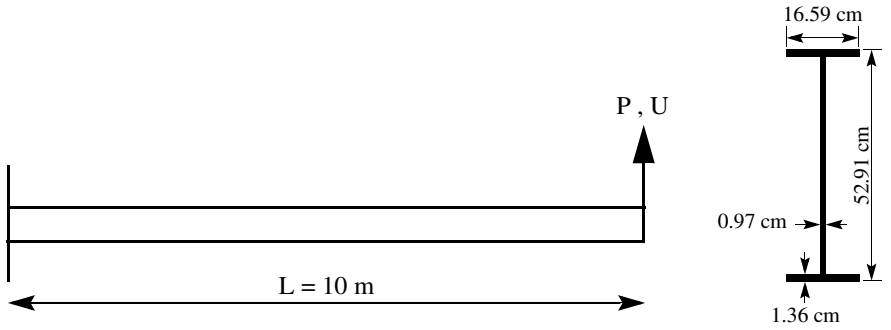


Fig. 3. Cantilever beam model: geometry, applied load and global response quantity.

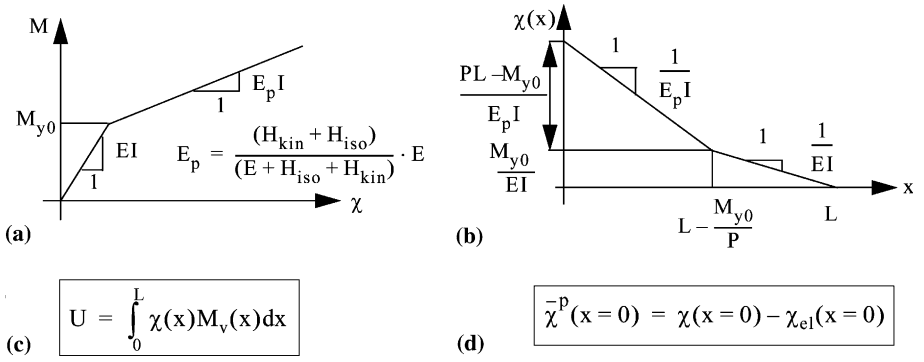


Fig. 4. Cantilever beam model: (a) moment–curvature relation ($J_2$ plasticity), (b) actual curvature ($\chi$) distribution, (c) computation of vertical tip displacement ($M_v(x)$: virtual moment) and (d) computation of cumulative plastic curvature at the fixed end.

$$\frac{\mathrm{d}U}{\mathrm{d}H_{\mathrm{kin}}} = \begin{cases} 0; & \text{if } P \leqslant \dfrac{M_{y0}}{L}, \\ -\dfrac{1}{6H_{\mathrm{kin}}^2 I}\left[2PL^3 - 3M_{y0}L^2 + \dfrac{M_{y0}^3}{P^2}\right]; & \text{if } P > \dfrac{M_{y0}}{L}. \end{cases} \tag{38}$$

The fixed end cumulative plastic curvature sensitivities to material parameters $E$, $M_{y0}$, and $H_{\mathrm{kin}}$ are derived as

$$\frac{\mathrm{d}\bar{\chi}^{\mathrm{p}}}{\mathrm{d}E} = 0, \tag{39}$$

$$\frac{\mathrm{d}\bar{\chi}^{\mathrm{p}}}{\mathrm{d}M_{y0}} = \begin{cases} 0; & \text{if } P \leqslant \dfrac{M_{y0}}{L}, \\ -\dfrac{1}{H_{\mathrm{kin}} I}; & \text{if } P > \dfrac{M_{y0}}{L}, \end{cases} \tag{40}$$

$$\frac{\mathrm{d}\bar{\chi}^{\mathrm{p}}}{\mathrm{d}H_{\mathrm{kin}}} = \begin{cases} 0; & \text{if } P \leqslant \dfrac{M_{y0}}{L}, \\ -\dfrac{PL - M_{y0}}{H_{\mathrm{kin}}^2 I}; & \text{if } P > \dfrac{M_{y0}}{L}. \end{cases} \tag{41}$$

Convergence analysis studies for the response quantities considered and their sensitivities to material parameters are performed using different meshes of force-based (F-B) elements (Figs. 5–12, part (a)) and of displacement-based (D-B) elements (Figs. 5–12, part (b)). The frame elements used follow Euler–Bernoulli beam theory (i.e., beam cross-sections remain plane and perpendicular to the beam centroidal axis) with linear geometry (i.e., small deformations and small strains). In the case of the D-B element, the common third-degree Hermitian polynomials are used as shape functions for the transverse displacement field, while the axial displacement shape functions are linear. In the case of the F-B element, the internal bending moment and axial force are interpolated exactly through a linear and a constant force field shape function, respectively, in the absence of element distributed loads.

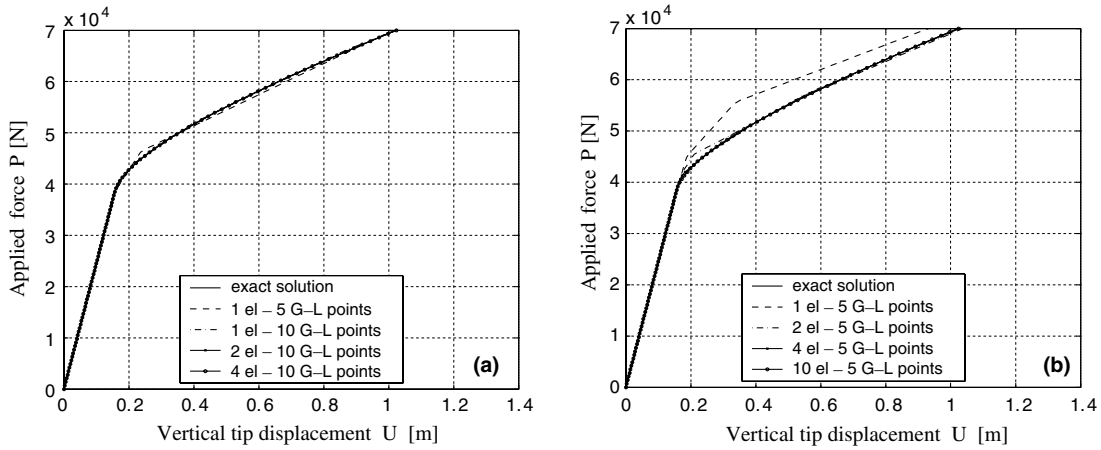


Fig. 5. Global response of the cantilever beam models: vertical tip displacement $U$; (a) force-based element models and (b) displacement-based element models.

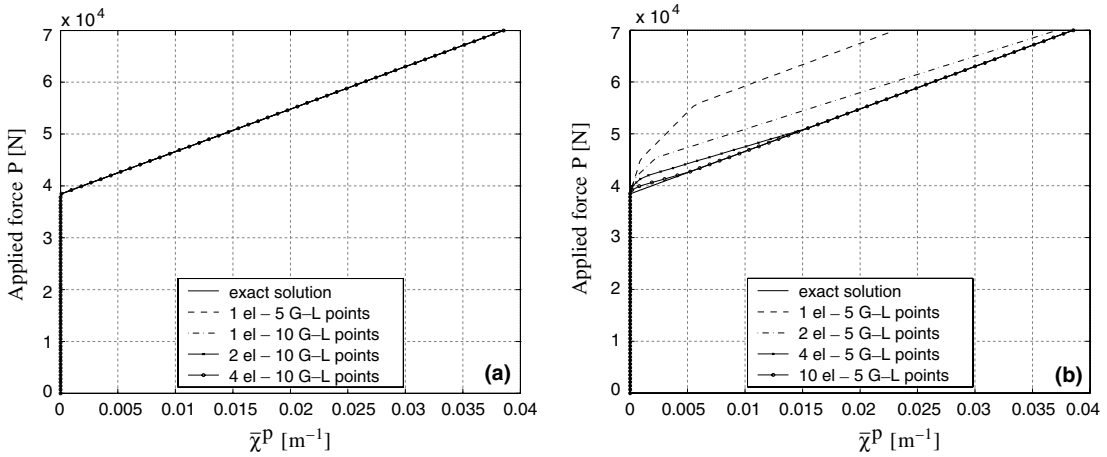


Fig. 6. Local response of the cantilever beam models: cumulative plastic curvature at the fixed end; (a) force-based element models and (b) displacement-based element models.

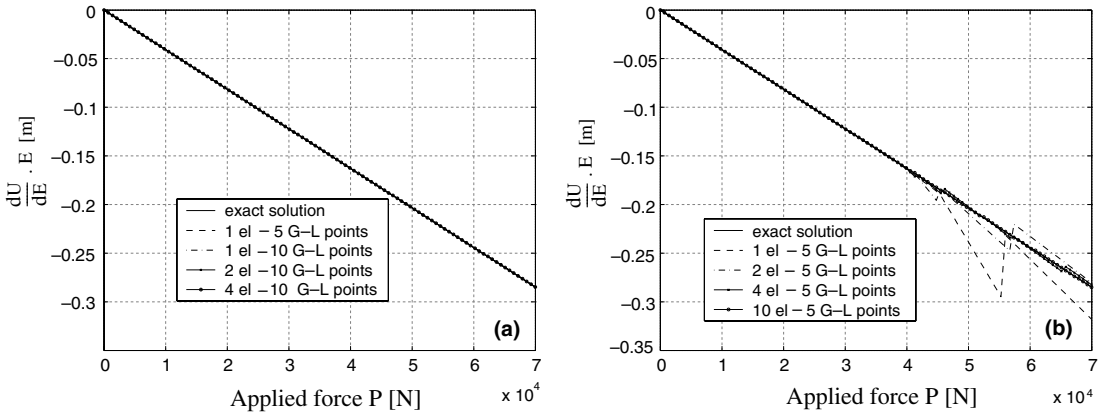


Fig. 7. Global response sensitivity of the cantilever beam models to Young's modulus $E$: (a) force-based element models and (b) displacement-based element models.

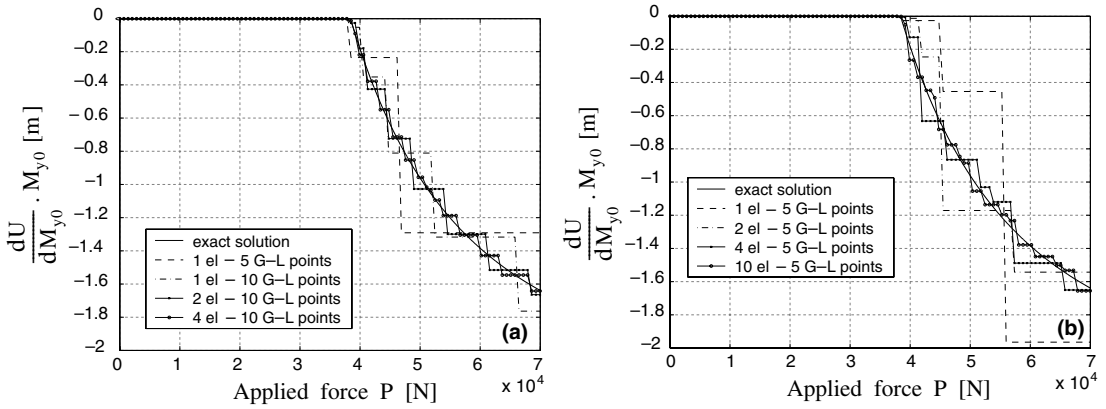


Fig. 8. Global response sensitivity of the cantilever beam models to the initial yield moment $M_{y0}$: (a) force-based element models and (b) displacement-based element models.

The finite element meshes considered for the F-B element models of the cantilever structure are: (a) one element with five Gauss–Lobatto (G–L) integration points along the length of the element, (b) one element with 10 G–L points, (c) two elements with 10 G–L points each and (d) four elements with 10 G–L points each. Those considered for the D-B element models of the cantilever beam are: (a) one element with five G–L points, (b) two elements with five G–L points each, (c) four elements with five G–L points each and (d) 10 elements with five G–L points each. The choice of the meshes was based on the objective of making, from the two sets of models (F-B and D-B), fair comparisons between the F-B and D-B results in terms of accuracy and computational effort. The selection of different numbers of Gauss–Lobatto integration points for the more refined meshes of the two kinds of elements is justified by the fact that increasing the number of integration points along the length of a F-B element improves significantly the accuracy of the results, at a slightly lower computational effort than by augmenting the number of F-B elements with a constant number of integration points per element. This is not the case of D-B elements, for which the error is produced mainly by the displacement interpolation shape functions that do not represent exactly the solution of

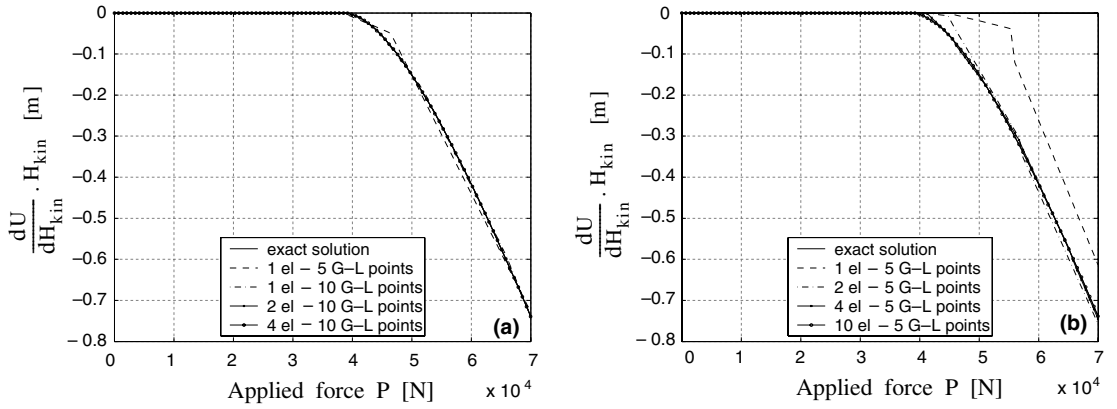


Fig. 9. Global response sensitivity of the cantilever beam models to the kinematic hardening modulus $H_{kin}$: (a) force-based element models and (b) displacement-based element models.

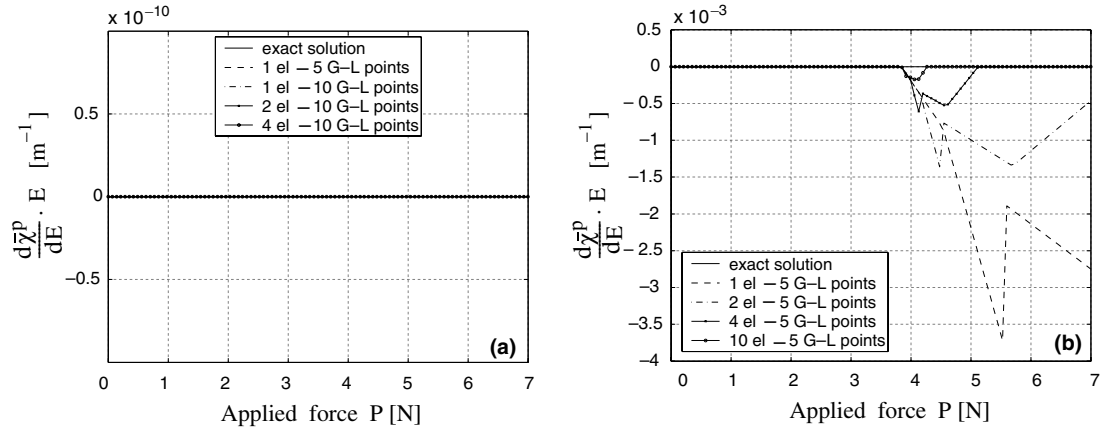


Fig. 10. Local response sensitivity of the cantilever beam models to Young's modulus $E$: (a) force-based element models and (b) displacement-based element models.

non-linear problems, and not by the approximate numerical integration. Thus in the case of D-B element models, for improving the accuracy of the results, it is more advantageous to increase the number of elements for a fixed total number of integration points. In the sequel, the 1 F-B element model with 10 G–L points is used as reference finite element model.

Figs. 5 and 6 show the convergence analysis results for the global and local response quantities, respectively. It is evident that the convergence (with increasing resolution of the finite element mesh) of the F-B element models toward the exact solution is much faster than the convergence of the D-B element models. Furthermore, for the D-B elements the local response results are less accurate than the global response results, while for the F-B elements the same level of accuracy is achieved for the global and local responses. It is observed that convergence to the exact solution is practically achieved for both the global and local responses using one F-B element with 10 G–L points, while four D-B elements (five G–L points each) are

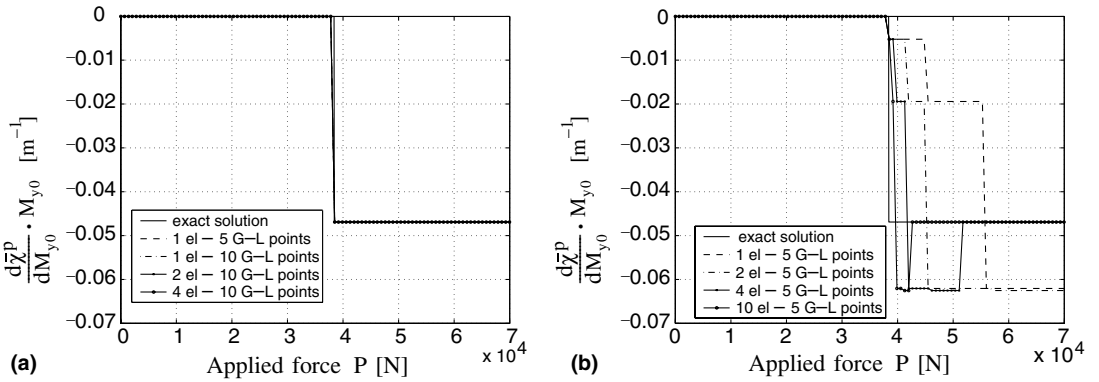


Fig. 11. Local response sensitivity of the cantilever beam models to the initial yield moment $M_{y0}$: (a) force-based element models and (b) displacement-based element models.

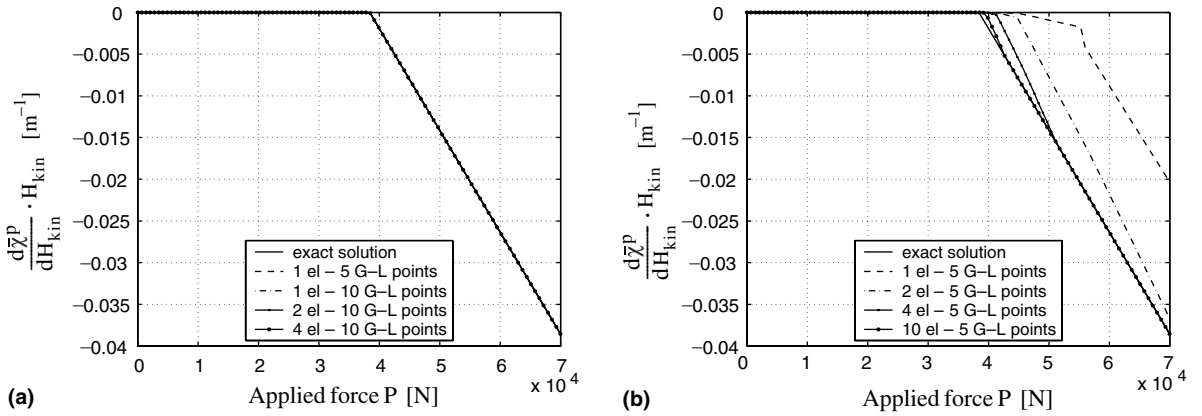


Fig. 12. Local response sensitivity of the cantilever beam models to the kinematic hardening modulus $H_{kin}$: (a) force-based element models and (b) displacement-based element models.

needed to predict accurately the global response quantity and 10 D-B elements (five G–L points each) produce fairly accurate results (but not as accurate as one F-B element with 10 G–L points) for the local response.

Figs. 7–9 display the tip displacement sensitivities to material parameters $E$, $M_{y0}$, and $H_{kin}$, respectively. The convergence trends are very similar to the ones obtained for the tip displacement response itself for both F-B and D-B element models. The sensitivities of the local response parameter $\overline{\chi}^{p}$ to material parameters $E$,$M_{y0}$, and $H_{kin}$ are displayed in Figs. 10–12, respectively. Again, the convergence trends are very similar to the ones found for the local response itself. Convergence to the exact solution is already achieved using one F-B element with five G–L points, while a 10 D-B element model with five G–L points per element produces sensitivity results with a non-negligible deviation from the exact solution.

It is noteworthy that small relative errors in the finite element response results can magnify into large relative errors in the response sensitivity results. This important remark is illustrated by comparing parts (a) and (b) of Figs. 6 and 11. In particular, the 10 D-B element model (with five G–L points/element) produces very accurate global response and global response sensitivity results (see parts (b) of Figs. 5, 7–9), and

also more than satisfactory results for the cumulative plastic curvature at the fixed end of the cantilever beam (see Fig. 6(b)), for which the error measure defined as the ratio between the maximum absolute error and the maximum absolute value is $\max |(\overline{\chi}^{p})_{FE} - (\overline{\chi}^{p})_{exact}| / \max |(\overline{\chi}^{p})_{exact}| = 0.0261$. Nevertheless, the same model produces large errors in the local response sensitivity to the initial yield moment, $M_{y0}$, at the load steps following the first yield excursion at the fixed end section, with an error measure of $\max |(\frac{d\overline{\chi}^{p}}{dM_{y0}})_{FE} - (\frac{d\overline{\chi}^{p}}{dM_{y0}})_{exact}| / \max |(\frac{d\overline{\chi}^{p}}{dM_{y0}})_{exact}| = 0.8889$. For the reference model (one F-B element with 10 G–L points), these error measures are $\max |(\overline{\chi}^{p})_{FE} - (\overline{\chi}^{p})_{exact}| / \max |(\overline{\chi}^{p})_{exact}| = 1.8 \times 10^{-15}$ and $\max |(\frac{d\overline{\chi}^{p}}{dM_{y0}})_{FE} - (\frac{d\overline{\chi}^{p}}{dM_{y0}})_{exact}| / \max |(\frac{d\overline{\chi}^{p}}{dM_{y0}})_{exact}| = 9.78 \times 10^{-14}$, respectively. The ratio of the maximum absolute error to the maximum absolute value has been preferred to other error measures (such as the maximum relative error) in order to avoid accounting for large errors caused by very small values of the quantity in question.

Fig. 13 provides the relative computing time (RCT), defined as the ratio of the computing time for a given finite element model to that of the reference model, for the various finite element models considered in this study. The model consisting of 1 F-B element with 10 G–L integration points is used as reference model since it achieves the best compromise between accuracy and computational effort. Among the D-B element models, an accuracy similar to that of the reference model is achieved by the four elements—five G–L points model (RCT = 1.33) for the response quantities and by the 10 elements—five G–L points model (RCT = 3.11) for the response sensitivities, excluding the fixed-end cumulative plastic curvature sensitivity to the initial yield moment $\frac{d\overline{\chi}^{p}}{dM_{y0}}$ as discussed earlier. Reducing the error in the computation of the latter response sensitivity using D-B elements is extremely difficult and requires very refined meshes near the fixed-end of the cantilever beam for at least two reasons: (a) because of the non-smoothness of the constitutive law used herein (i.e., the non-smoothness of the 1-D $J_2$ plasticity model contributes to magnifying further small errors in the response results into large errors in the corresponding response sensitivities), and (b) because of the intrinsic error in the D-B formulation in representing the force distribution along the element.

From this section, it can be concluded that the benefits of using F-B element models are evident: they achieve more accurate response and response sensitivity results at a lower computational cost. The comparative results between F-B and D-B elements obtained here for response computation are consistent with those obtained by previous researchers (see [12–15]). The advantages of the force-based over the displacement-based elements for response computation are amplified for response sensitivity computation.

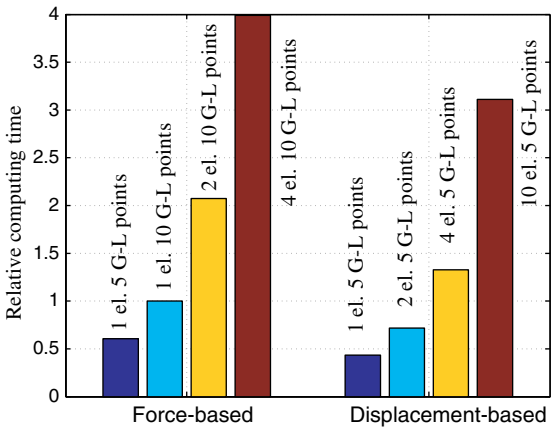


Fig. 13. Relative computing times for the cantilever beam models (reference model taken as the one F-B element with 10 G–L points).

### 4.2. Application example: statically indeterminate 2-D frame with distributed plasticity

The second structure used as application example is the single-storey, single-bay statically indeterminate steel frame with pin supports shown in Fig. 14. The cross-section and material properties are the same as in the previous example.

The simple case of a monotonically increasing horizontal point load applied at roof level is considered. The resulting horizontal nodal displacement $U$ (see Fig. 14) can be derived in closed-form from the principle of virtual forces (dummy unit load principle) as (Fig. 15)

$$U = \int_{\text{str}} \chi(x) M_v(x) \mathrm{d}x + \int_{\text{str}} \varepsilon(x) N_v(x) \mathrm{d}x, \tag{42}$$

where $\chi(x)$ and $\varepsilon(x)$ denote the actual curvature and axial strain along the beam axis $x$, respectively, and $M_v(x)$ and $N_v(x)$ represent the virtual moment and axial force, respectively, due to the dummy unit load. In this example, we consider the roof horizontal displacement $U$ as global response quantity and the cumulative plastic curvature, $\overline{\chi}^{\text{p}}$, in the section at the top of the left column (see Fig. 14) as local response quantity. The analytical solutions for these two response quantities have been derived as

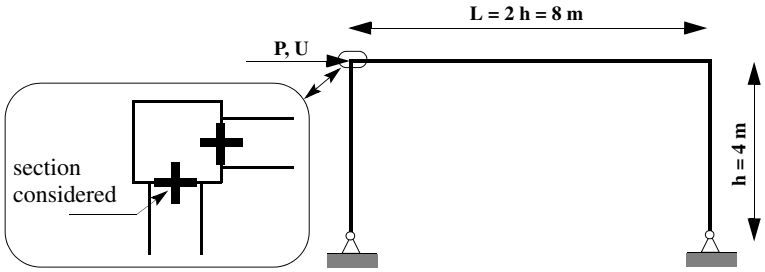


Fig. 14. Statically indeterminate frame model: geometry, applied loads and global response quantity.

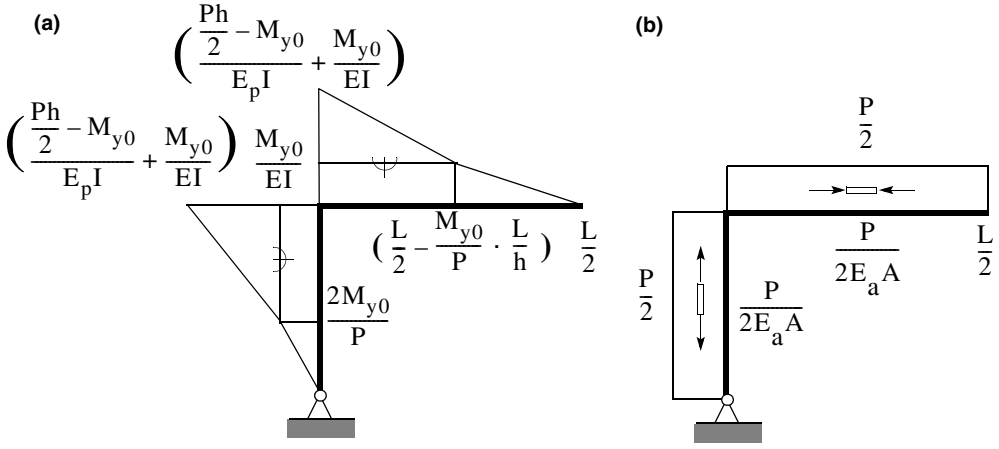


Fig. 15. Statically indeterminate frame: (a) actual curvature distribution, and (b) actual axial force and axial deformation distributions (due to symmetry of the problem, only half of the frame is represented).

$$U = \begin{cases} \dfrac{Ph^3}{6EI}\left(1+\dfrac{L}{2h}\right)+\dfrac{PL}{4E_aA}\left[1+\left(\dfrac{2h}{L}\right)^3\right]; & \text{if } P \leqslant \dfrac{2M_{y0}}{h}, \\ \left[\dfrac{Ph^3}{6EI}\left(1+\dfrac{E}{H_{\text{kin}}}\right)-\dfrac{M_{y0}h^2}{2H_{\text{kin}}I}+\dfrac{2M_{y0}^3}{3P^2H_{\text{kin}}I}\right]\left(1+\dfrac{L}{2h}\right)+\dfrac{PL}{4E_aA}\left[1+\left(\dfrac{2h}{L}\right)^3\right]; & \text{if } P > \dfrac{2M_{y0}}{h}, \end{cases} \tag{43}$$

$$\bar{\chi}^p = \begin{cases} 0; & \text{if } P \leqslant \dfrac{2M_{y0}}{h}, \\ \dfrac{Ph-2M_{y0}}{2H_{\text{kin}}I}; & \text{if } P > \dfrac{2M_{y0}}{h}, \end{cases} \tag{44}$$

where the Young's modulus for the linear elastic axial behavior is referred to as $E_a$, while Young's modulus for the flexural behavior is denoted by $E$.

The roof horizontal displacement sensitivities to material parameters $E$, $M_{y0}$, and $H_{\text{kin}}$ are derived in closed-form from Eq. (43) as

$$\frac{\mathrm{d}U}{\mathrm{d}E} = -\frac{Ph^3}{6E^2I}\left(1+\frac{L}{2h}\right), \tag{45}$$

$$\frac{\mathrm{d}U}{\mathrm{d}M_{y0}} = \begin{cases} 0; & \text{if } P \leqslant \dfrac{2M_{y0}}{h}, \\ -\dfrac{1}{2H_{\text{kin}}I}\left[h^2-\left(\dfrac{2M_{y0}}{P}\right)^2\right]\left(1+\dfrac{L}{2h}\right); & \text{if } P > \dfrac{2M_{y0}}{h}, \end{cases} \tag{46}$$

$$\frac{\mathrm{d}U}{\mathrm{d}H_{\text{kin}}} = \begin{cases} 0; & \text{if } P \leqslant \dfrac{2M_{y0}}{h}, \\ -\dfrac{1}{6H_{\text{kin}}^2I}\left[Ph^3-3M_{y0}h^2+\dfrac{4M_{y0}^3}{P^2}\right]\left(1+\dfrac{L}{4h}\right); & \text{if } P > \dfrac{2M_{y0}}{h}. \end{cases} \tag{47}$$

The sensitivities of the cumulative plastic curvature (at the cross-section shown in Fig. 14) to the same material parameters $E$, $M_{y0}$, and $H_{\text{kin}}$ are obtained in closed-form from Eq. (44) as

$$\frac{\mathrm{d}\bar{\chi}^p}{\mathrm{d}E} = 0, \tag{48}$$

$$\frac{\mathrm{d}\bar{\chi}^p}{\mathrm{d}M_{y0}} = \begin{cases} 0; & \text{if } P \leqslant \dfrac{2M_{y0}}{h}, \\ -\dfrac{1}{H_{\text{kin}}I}; & \text{if } P > \dfrac{2M_{y0}}{h}, \end{cases} \tag{49}$$

$$\frac{\mathrm{d}\bar{\chi}^p}{\mathrm{d}H_{\text{kin}}} = \begin{cases} 0; & \text{if } P \leqslant \dfrac{2M_{y0}}{h}, \\ -\dfrac{Ph-2M_{y0}}{2H_{\text{kin}}^2I}; & \text{if } P > \dfrac{2M_{y0}}{h}. \end{cases} \tag{50}$$

It is worth noting that the contribution of the axial deformation to the horizontal roof displacement $U$ (very small compared to the flexural one, but not negligible) does not appear in the response sensitivities, because they are computed with respect to the $J_2$ plasticity constitutive law parameters, which effect only the flexural behavior.

The frame elements used in this second application example are the same as in the first one. The F-B element model meshes are: (a) three elements with five G–L integration points each (one element for each column and beam), (b) three elements with 10 G–L points each (one element for each column and beam), (c) six elements with 10 G–L points each (two elements for each column and beam), and (d) 12 elements with 10 G–L points each (four elements for each column and beam). The D-B element model meshes are: (a) three elements with five G–L integration points each (one element for each column and beam), (b) six elements with five G–L points each (two elements for each column and beam), (c) 12 elements with five G–L points each (four elements for each column and beam), and (d) 40 elements with five G–L points each (10 elements for each column and 20 elements for the beam). The three F-B element model with 10 G–L points each is taken as the reference model in defining the relative computational efforts.

Also the presentation of the convergence analysis results emphasizing the comparison between F-B and D-B element models is the same as in the previous example. Figs. 16 and 17 present results on the convergence of the global and local response quantities, respectively, for increasing resolution of the finite element mesh. Figs. 18–20 display the global response sensitivities to constitutive model parameters $E$, $M_{y0}$, and

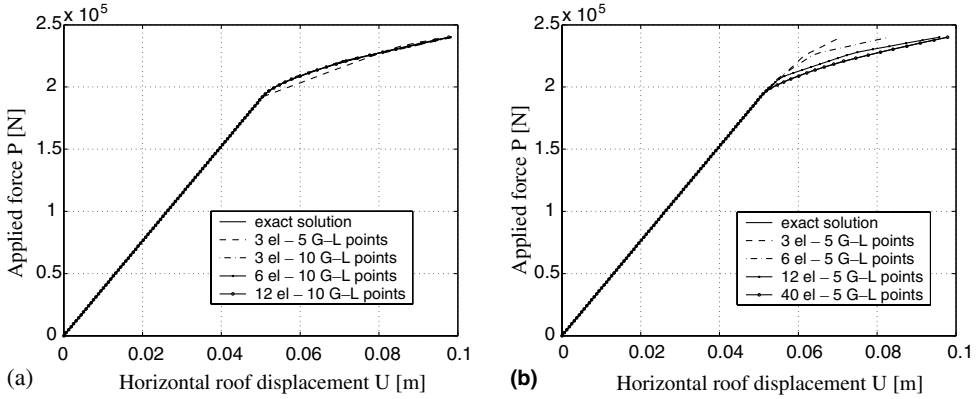


Fig. 16. Global response of the single-storey frame models: roof horizontal displacement $U$; (a) force-based element models and (b) displacement-based element models.

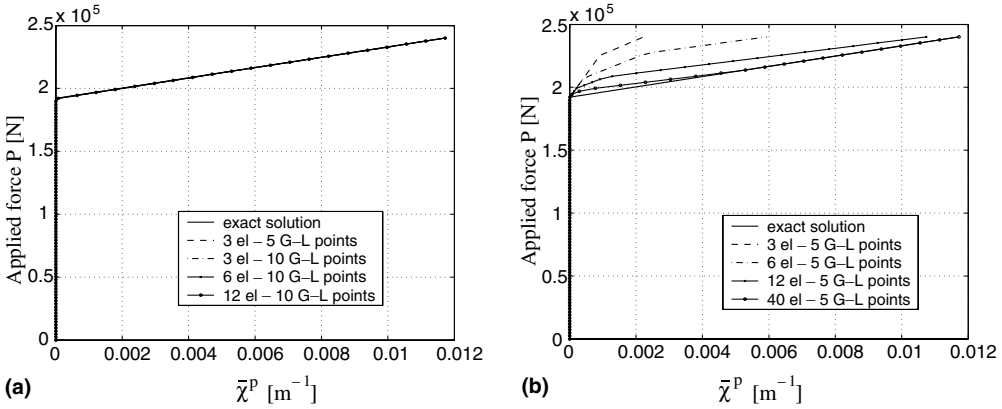


Fig. 17. Local response of the single-storey frame models: cumulative plastic curvature in the section at the top of the left column; (a) force-based element models and (b) displacement-based element models.

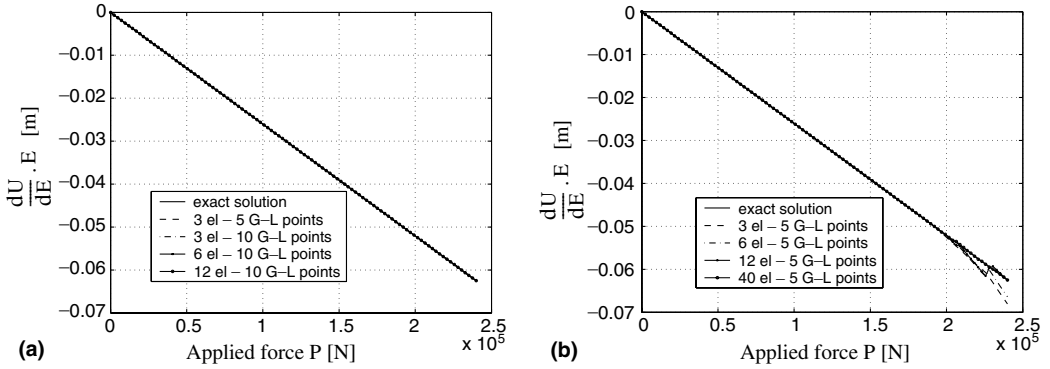


Fig. 18. Global response sensitivity of the single-storey frame models to Young's modulus $E$: (a) force-based element models and (b) displacement-based element models.

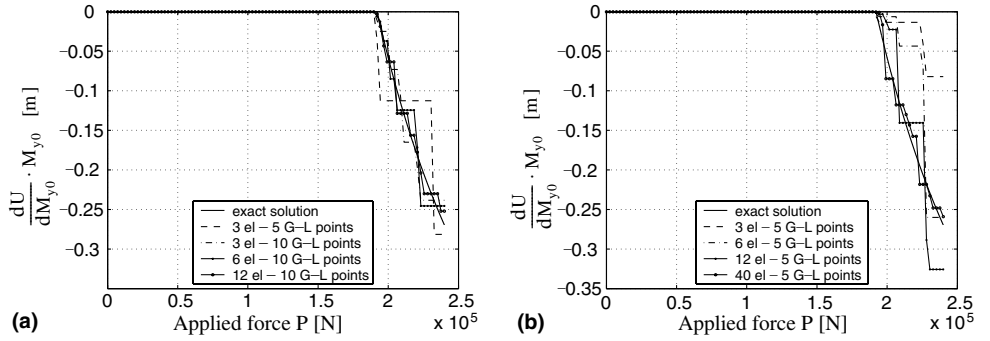


Fig. 19. Global response sensitivity of the single-storey frame models to the initial yield moment $M_{y0}$: (a) force-based element models and (b) displacement-based element models.

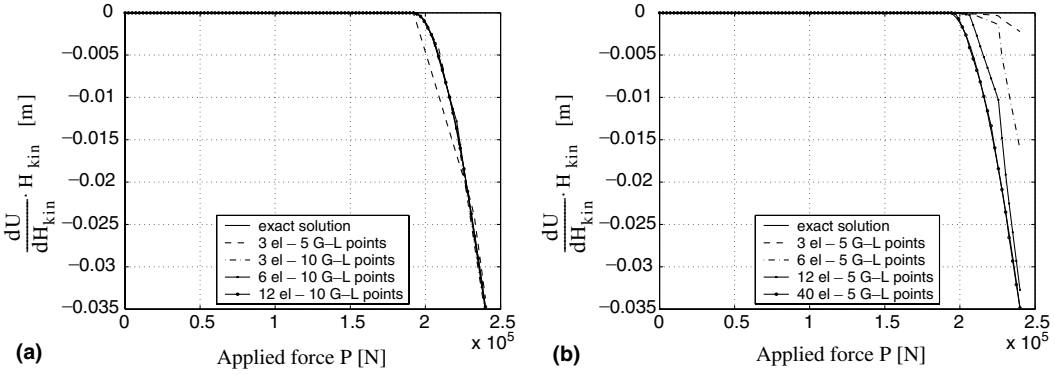


Fig. 20. Global response sensitivity of the single-storey frame models to the kinematic hardening modulus $H_{\text{kin}}$: (a) force-based element models and (b) displacement-based element models.

$H_{\text{kin}}$, while Figs. 21–23 show the local response sensitivities to these same material parameters. Finally, Fig. 24 provides the relative computing times for the finite element meshes defined above.

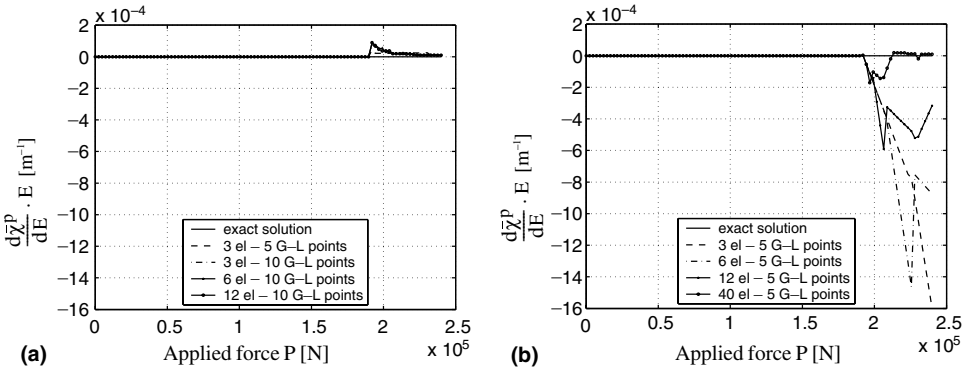


Fig. 21. Local response sensitivity of the single-storey frame models to Young's modulus $E$: (a) force-based element models and (b) displacement-based element models.

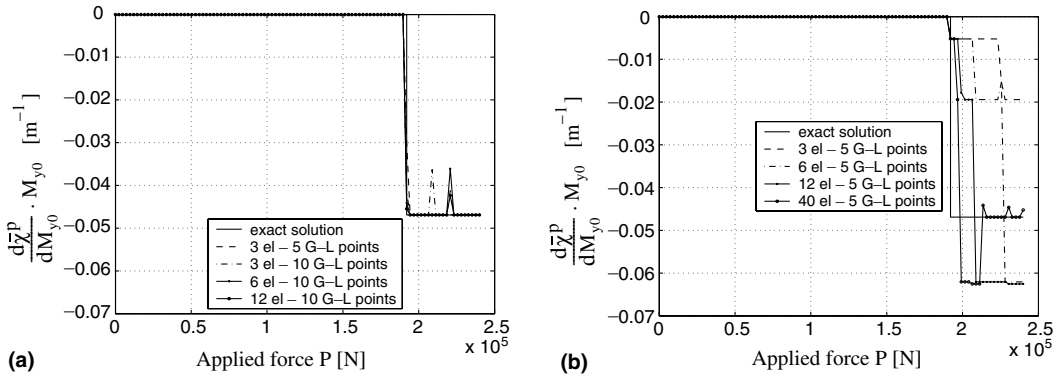


Fig. 22. Local response sensitivity of the single-storey frame models to the initial yield moment $M_{y0}$: (a) force-based element models and (b) displacement-based element models.

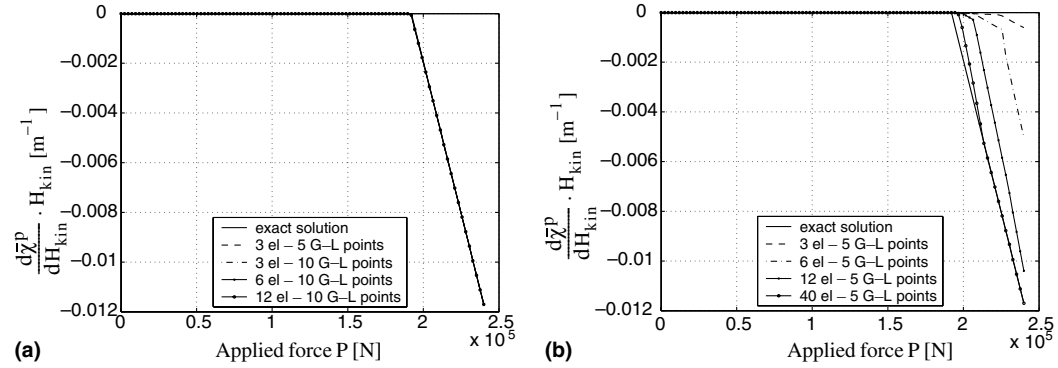


Fig. 23. Local response sensitivity of the single-storey frame models to the kinematic hardening modulus $H_{\mathrm{kin}}$: (a) force-based element models and (b) displacement-based element models.

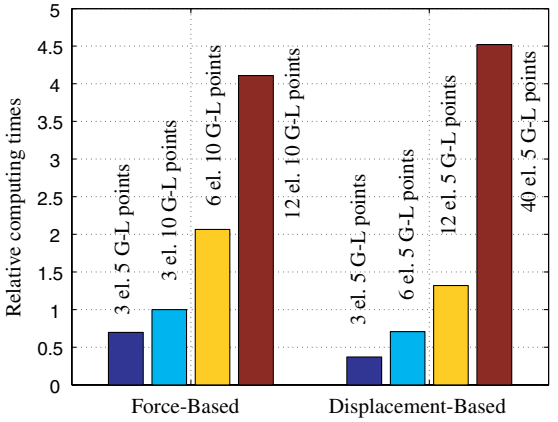


Fig. 24. Relative computing times for the single-storey frame models (reference model taken as the three F-B elements with 10 G–L points each).

The results obtained here are consistent with those obtained in the previous example. However, some further remarks can be made from this second case study.

(a) The convergence toward the exact solution of the D-B element models is much slower than for the cantilever beam example, while the F-B element models provide similar accuracy in both cases. This could be expected due to the more complex flexural behavior (i.e., change of sign of curvature) of the beam in the frame, which is correctly captured with the force formulation, but not with the displacement formulation.
(b) The response sensitivity convergence results of the D-B element models are even worse than the response convergence results when comparing the cantilever beam and frame examples. Again, response sensitivity convergence results for F-B elements are similar for both examples (e.g., local response sensitivity results already practically converge using one 1 F-B element with five G–L points per beam or column in both examples).
(c) A more refined mesh (not any more with a constant number of finite elements per structural element) is required with D-B elements to achieve an accuracy approaching that of the reference model (three F–B elements with 10 G–L points each). For this example, the D-B element model with similar accuracy to that of the reference model is the 40 elements with five G–L points each (10 elements per column and 20 elements for the beam). This model however has a relative computing time of 4.52.

The advantage in using F-B element models (over D-B element models) for response sensitivity analysis is even more significant than in the previous example. It is believed, from theoretical considerations and from the above application examples, that this benefit in terms of improved accuracy at a lower computational cost increases with the complexity of the structural system being analyzed.

### *4.3. Application example: statically indeterminate five-storey, one-bay 2-D frame with distributed plasticity*

The third test structure considered in this comparative study is a five-storey, single-bay steel moment resisting frame, a finite element model of which is shown in Fig. 25. All columns and beams are W21 × 50 steel I-beams with an initial yield moment of $M_{y0}$ = 384.2 [kN m]. A 20% post-yield to initial flexural stiffness ratio is assumed. The axial behavior is assumed linear elastic, while the flexural behavior is

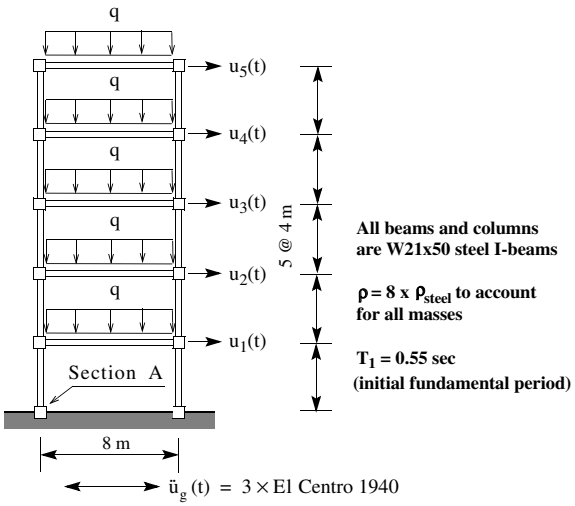


Fig. 25. Moment-resisting building frame model: geometry, gravity loads and floor displacements.

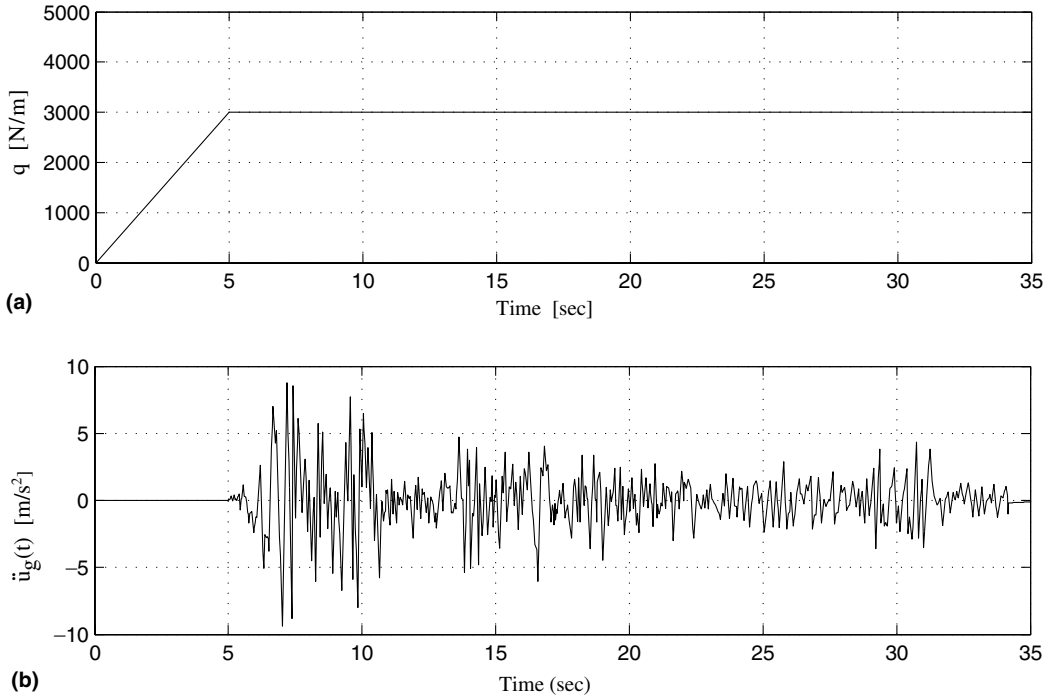


Fig. 26. Loading time histories for the dynamic analysis of the five storey building models: (a) gravity loads and (b) earthquake excitation.

described by a 1-D $J_2$ plasticity section constitutive law (see [5,6]) with the following material parameters: Young's modulus $E = 2 \times 10^8$ [kPa], and isotropic and kinematic hardening moduli $H_{iso} = 0$ [kPa], $H_{kin} = 5 \times 10^7$ [kPa], respectively. A material mass density of 8 times the mass density of steel (i.e.,

$\rho = 63200$ [kg/m$^3$]) is used for the beams only in order to account for typical additional masses (i.e., slabs, floor beams, ceilings,...) and for the mass of the columns.

The structure is modeled using the D-B and F-B frame elements described earlier in the paper. The inertia properties of the system are modeled through (translational) lumped masses (in both the horizontal and vertical directions) applied at the nodes of the finite elements representing the beams, each element contributing half of its total mass to each of its end nodes. No lumped masses are applied at the internal nodes of the columns, thus obtaining finite element models with mesh independent total inertia properties. The frame

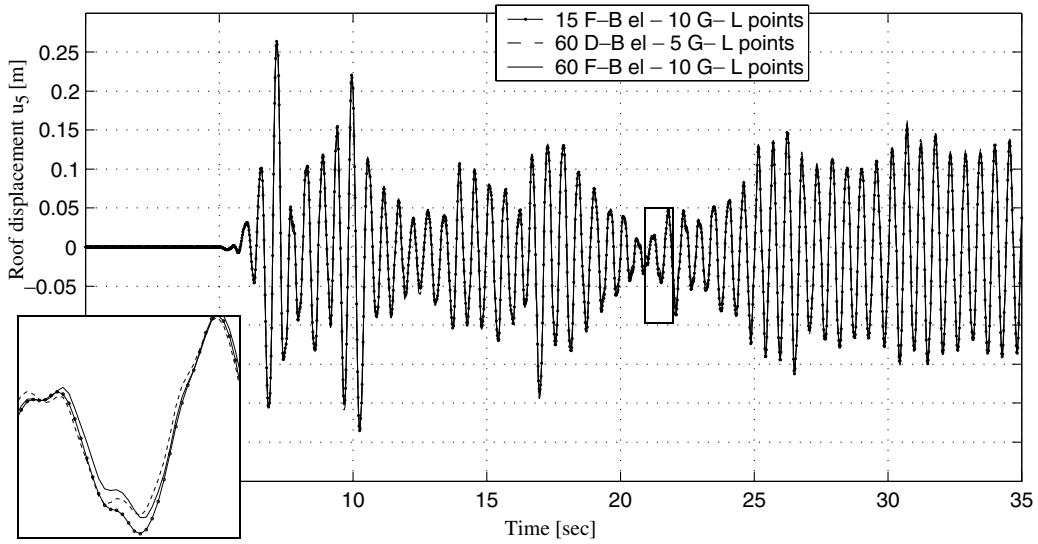


Fig. 27. Global response of the five storey building models for earthquake loading: roof displacement histories.

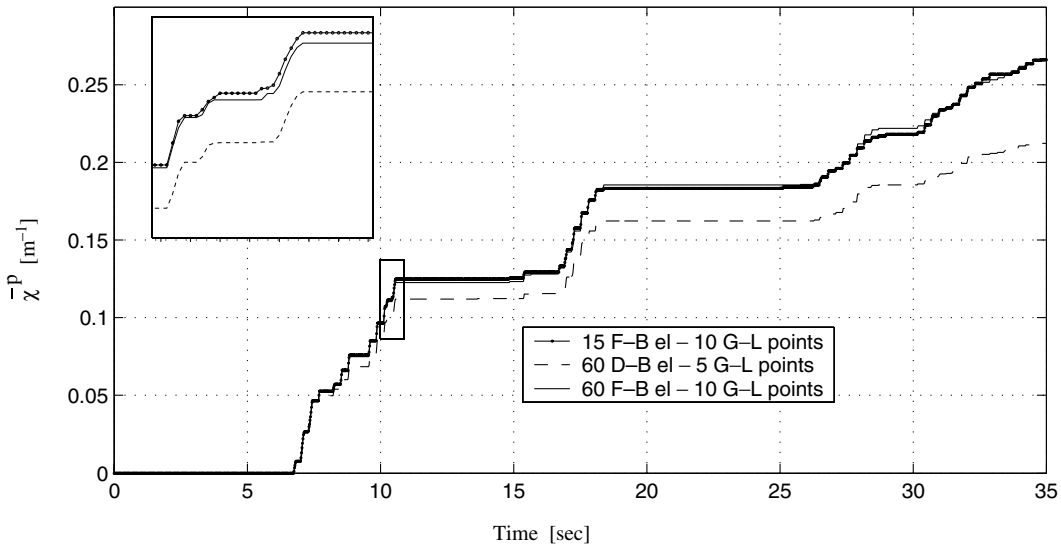


Fig. 28. Local response of the five storey building models for earthquake loading: cumulative plastic curvature histories at section A.

has an initial fundamental period of 0.55 s. No sources of energy dissipation (such as viscoelastic damping) beyond hysteretic energy dissipation through inelastic flexural action are considered here.

After application of gravity loads, this frame is subjected to a non-linear response history analysis for earthquake base excitation, taken as the balanced 1940 El Centro earthquake record scaled by a factor 3 (see Fig. 26). In this dynamic analysis, the unconditionally stable constant average acceleration method [3] with a constant time step of $\Delta t = 0.02$ s is used as time stepping scheme.

The frame element models compared here are: (a) 15 F-B elements (one frame element per column or beam) with 10 G–L points each and (b) 60 D-B elements (four frame elements per column or beam) with five G–L points each. The ratio of the computing time of the D-B element model over that of the F-B element model was found to be about 1.4.

There is no closed-form solution available for the present problem. Therefore, a reference model consisting of 60 F-B elements (four frame elements per column or beam) with 10 G–L points each was selected. Convergence toward the unknown exact solution has been verified with three different meshes (15 F-B elements, 30 F-B elements and 60 F-B elements, with 10 G–L points each). The response and response sensitivity results obtained from the reference model are believed to be the most accurate results. It is worth noting that with a lumped mass modeling, the refinement of the mass discretization (even for a constant total mass) may have a non-negligible influence on the convergence trend of the results. Further studies are required in order to evaluate this effect and to compare the convergence results based on lumped mass modeling with those based on consistent mass modeling of the distributed masses.

The time histories of significant global (roof horizontal displacement $u_5$) and local (cumulative plastic curvature $\bar{\chi}^p$ at the fixed section of the left base column, referred to as section A, see Fig. 25) response quantities are plotted in Figs. 27 and 28. Figs. 29–31 display the roof horizontal displacement sensitivities to Young's modulus, $E$, the initial yield moment, $M_{y0}$, and the kinematic hardening modulus, $H_{\text{kin}}$, respectively; while the sensitivities of the cumulative plastic curvature in section A to the material sensitivity parameters $E$, $M_{y0}$ and $H_{\text{kin}}$ are shown in Figs. 32–34, respectively. In Fig. 32, the sensitivity of the cumulative plastic curvature in section A to the material sensitivity parameter $E$ is also shown for the frame model consisting of 30 F-B

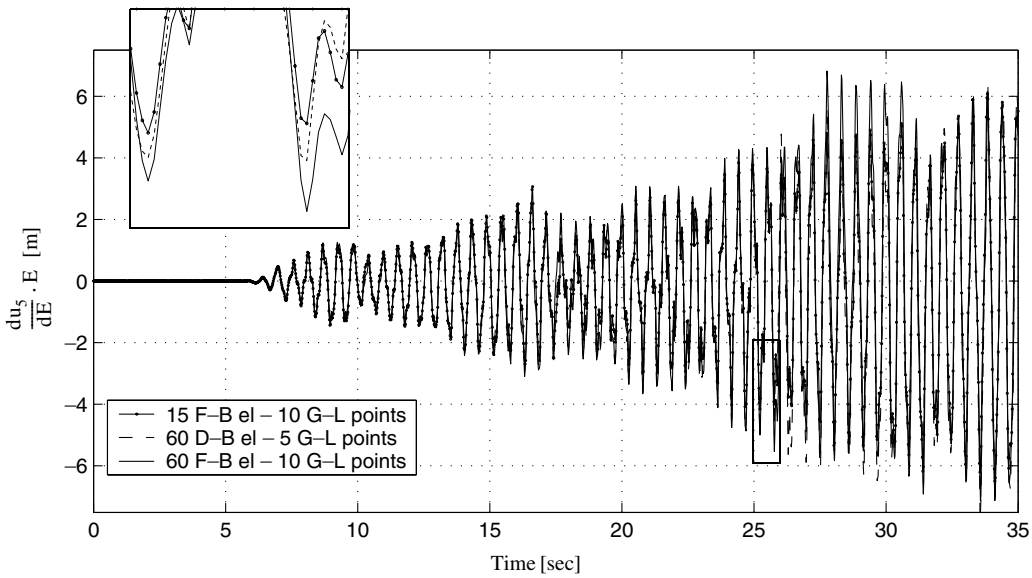


Fig. 29. Global response sensitivities of the five storey building models to material parameters: roof displacement sensitivity to Young's modulus, $E$.

elements with 10 G–L points each. Global and local response sensitivities to the ground motion acceleration value at time $t = 6.00$ s are plotted in Figs. 35 and 36, respectively. In Figs. 27–36, insets present closer views of the response and response sensitivity histories. Fig. 37 compares the error measures for the two response quantities considered and their sensitivities as computed using the F-B element model (15 and 30 F-B elements with 10 G–L points each) and the D-B element model (60 D-B elements with five G–L points each).

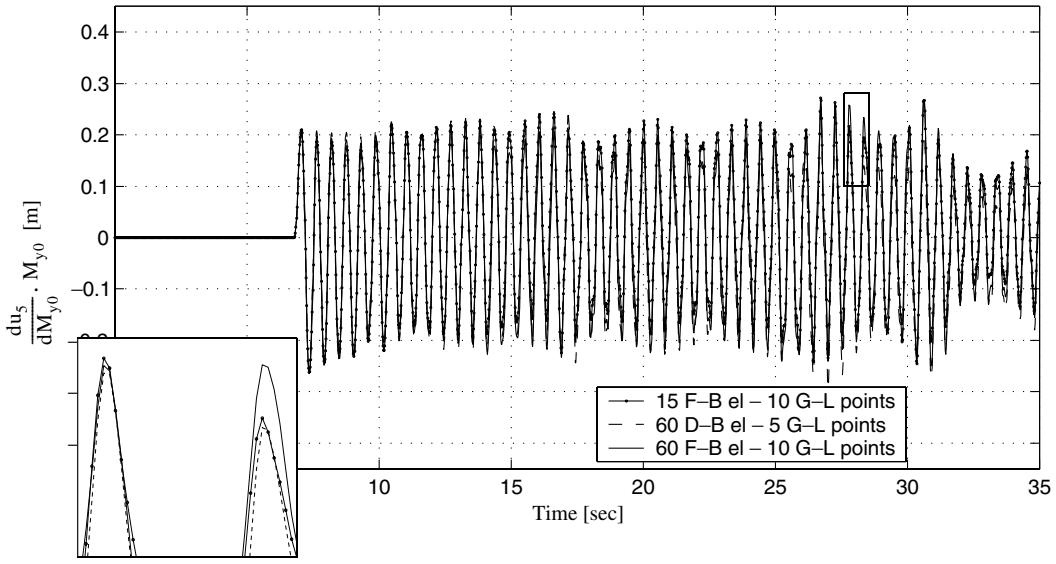


Fig. 30. Global response sensitivities of the five storey building models to material parameters: roof displacement sensitivity to the initial yield moment, $M_{y0}$.

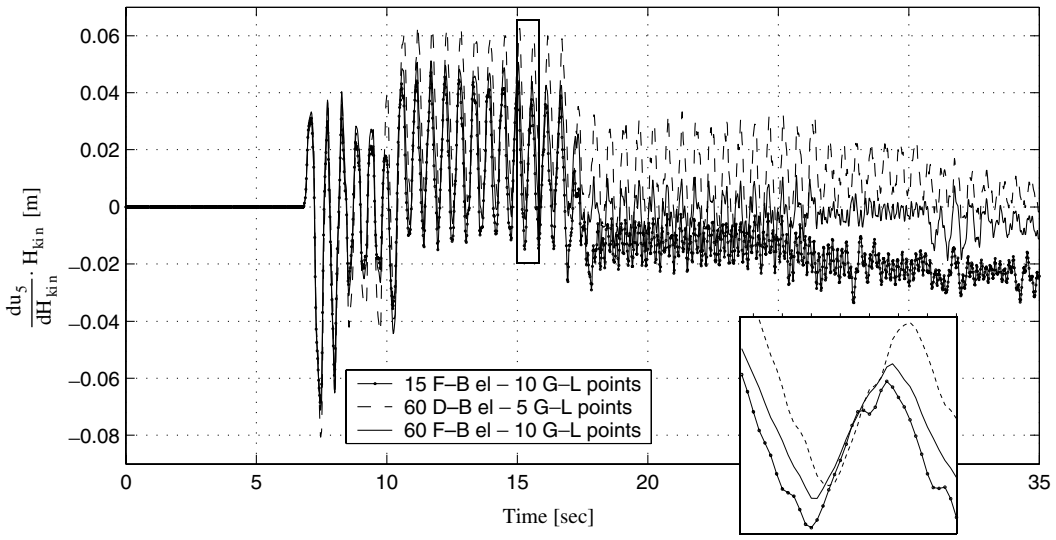


Fig. 31. Global response sensitivities of the five storey building models to material parameters: roof displacement sensitivity to the kinematic hardening modulus, $H_{\mathrm{kin}}$.

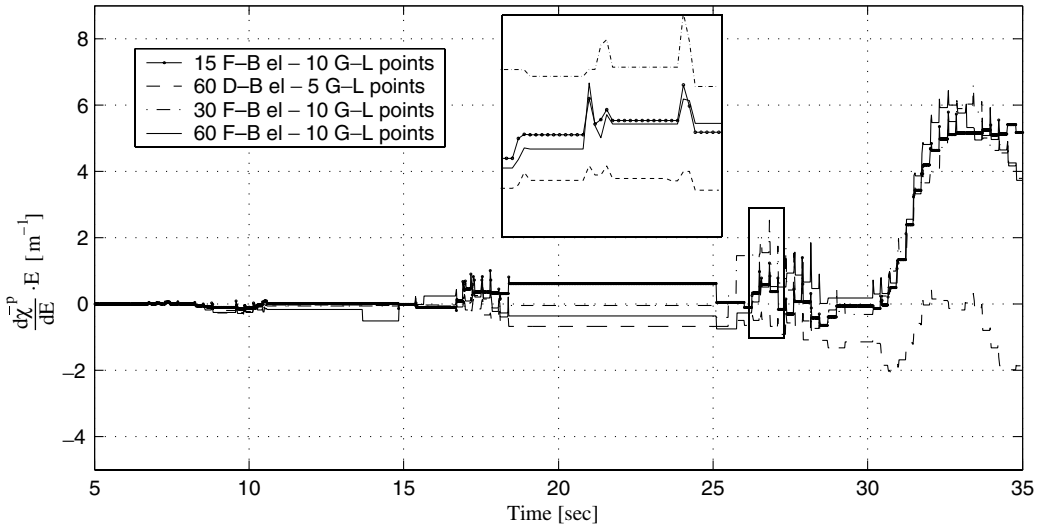


Fig. 32. Local response sensitivities of the five storey building models to material parameters: sensitivity of cumulative plastic curvature in section A to Young's modulus, $E$.

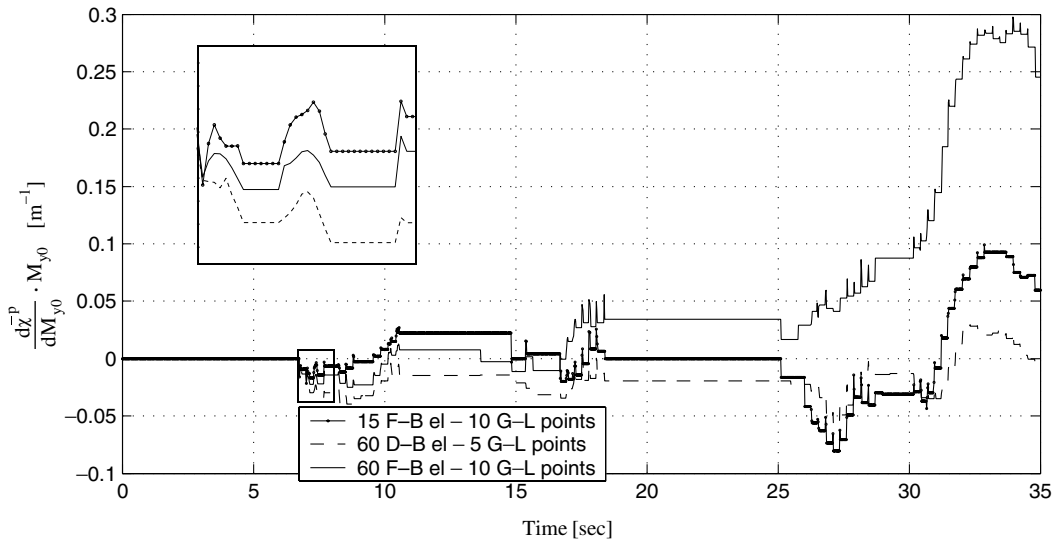


Fig. 33. Local response sensitivities of the five storey building models to material parameters: sensitivity of cumulative plastic curvature in section A to the initial yield moment, $M_{y0}$.

This figure shows that, except for response sensitivity $d\bar{\chi}_p/dE$, all responses and response sensitivities considered converge towards the corresponding results obtained from the reference model when the F-B element mesh is refined from 15 to 30 elements. For the case of the sensitivity of the cumulative plastic curvature in section A to the material sensitivity parameter $E$, $d\bar{\chi}_p/dE$, as shown in Fig. 32, the error for the 30 F-B elements with 10 G–L points each is smaller than the error for the 15 F-B element model, except during the time intervals [25.5–27]s and [32–34]s of the response history. Each of the response sensitivities presented above is

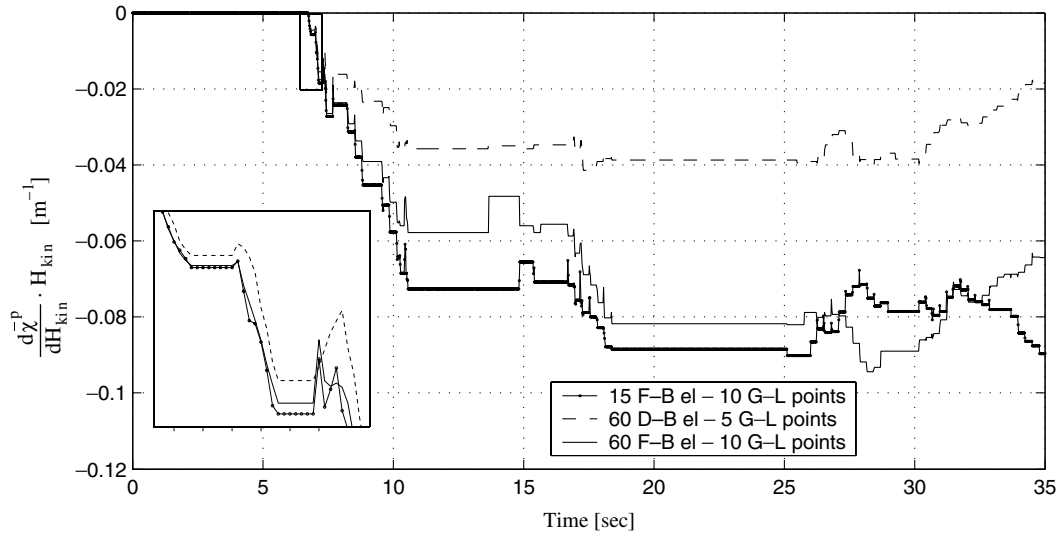


Fig. 34. Local response sensitivities of the five storey building models to material parameters: sensitivity of cumulative plastic curvature in section A to the kinematic hardening modulus, $H_{\text{kin}}$.

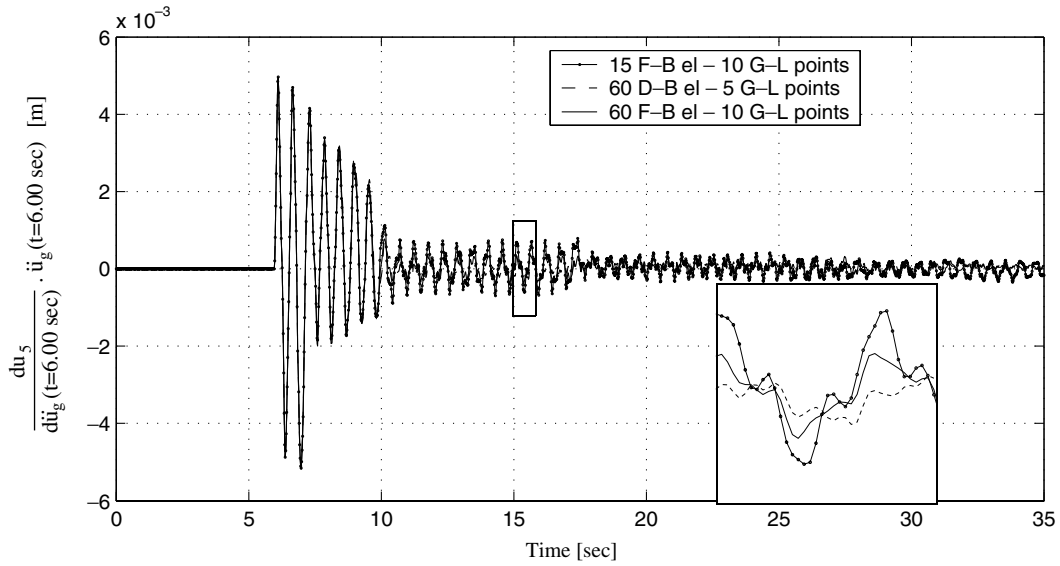


Fig. 35. Global response sensitivities of the five storey building models to loading parameters: roof displacement sensitivity to earthquake ground acceleration at time $t = 6.00\,\text{s}$.

scaled by the sensitivity parameter itself (i.e., $(\mathrm{d}r/\mathrm{d}\theta) \cdot \theta$) and can thus be interpreted as 100 times the change in the response quantity due to one percent change in the sensitivity parameter. These scaled sensitivities can therefore be used to determine the relative importance of the sensitivity parameters in regards to a given response quantity. Fig. 38 displays the maximum absolute values of the scaled response sensitivities to the sensitivity parameters considered in this study.

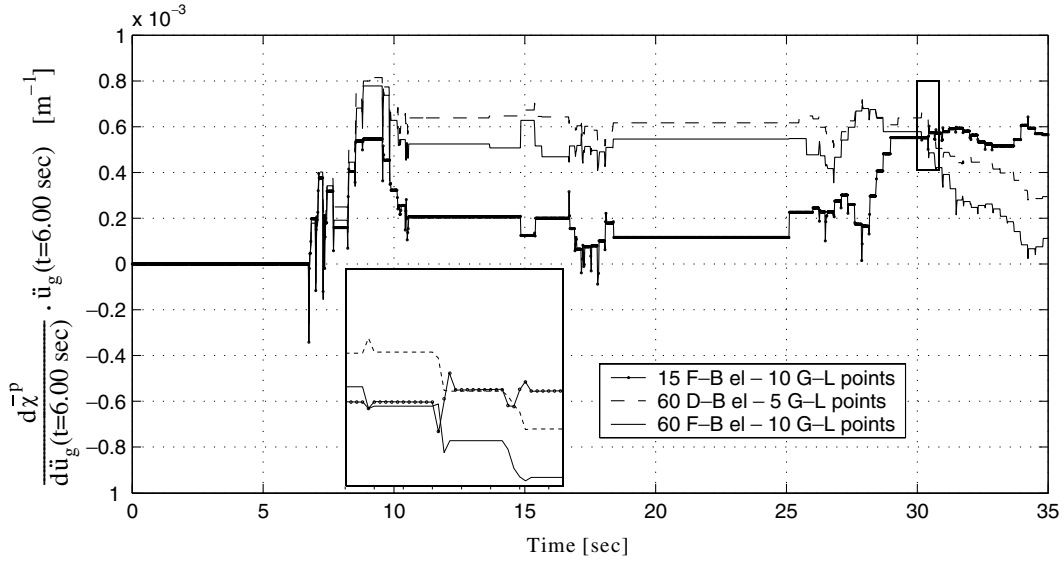


Fig. 36. Local response sensitivities of the five storey building models to loading parameters: sensitivity of cumulative plastic curvature in section A to earthquake ground acceleration at time $t = 6.00\,\mathrm{s}$.

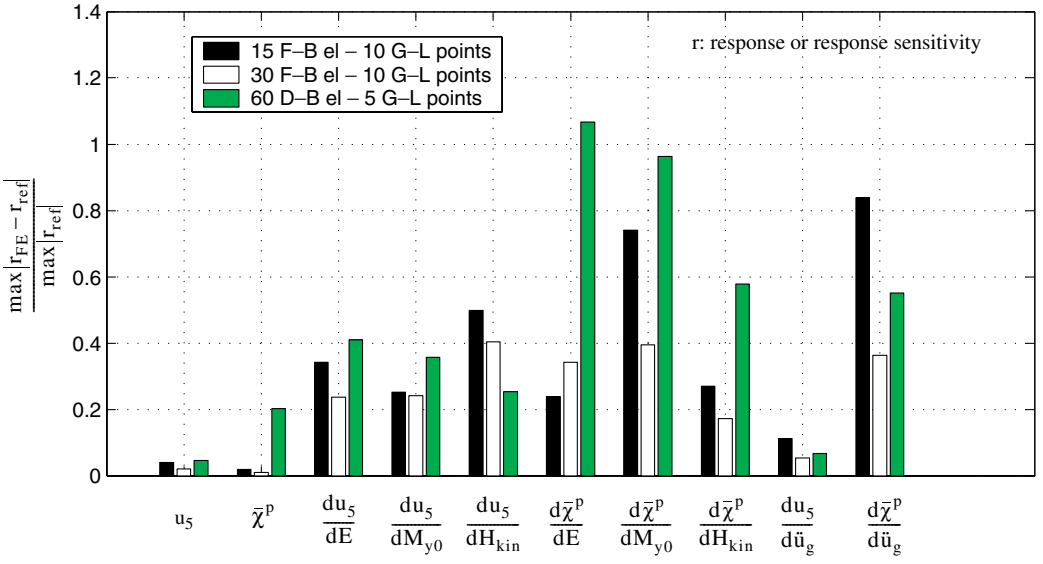


Fig. 37. Error measures for the five storey building models (reference model taken as the 60 F-B elements with 10 G–L points each).

The following new remarks can be made from the results described above.

(a) The computed global response quantities obtained from the two compared models are very close, while there are substantial differences between the local response quantities computed from these models.

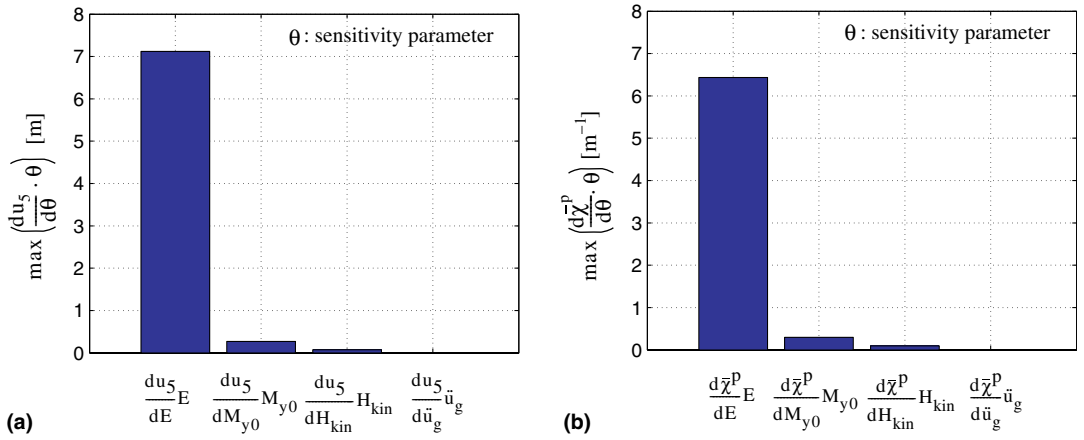


Fig. 38. Relative importance of the sensitivity parameters for the five storey building models: (a) for global response quantities and (b) for local response quantities.

(b) The global response sensitivities to material parameters, computed with the two compared models, are very similar, with a slightly better accuracy overall for the F-B model.
(c) The local response sensitivities to material parameters computed with the F-B model are much closer to the reference model results than those obtained from the D-B model.
(d) The D-B model provides more accurate global and local response sensitivities to the discrete loading parameter considered than the F-B model. However, this relative advantage of the D-B model may be due to its more accurate description of the distributed mass.
(e) According to the scaled sensitivity results presented in Fig. 38, the global and local response quantities considered here are most sensitive to Young's modulus, $E$, by a wide margin. This result depends mainly on the fact that changes in the stiffness properties produce a change in the natural periods of the structure, resulting in a gradually increasing shift in time between the response histories of the original and perturbed structures, respectively. This time shift produces large response sensitivities. The F-B model performs particularly well when used to evaluate the sensitivities of the global and local response quantities to Young's modulus.

This third example shows again that F-B element models perform better than D-B element models as they achieve better accuracy overall for both response and response sensitivities at a lower computational cost (here about 30% lower). This higher accuracy is particularly pronounced for the local response quantity considered and its sensitivities. Nevertheless, it is pointed out that higher performance of the F-B elements could possibly be achieved in dynamic cases through the development of a mass description consistent with the element formulation.

## 5. Insight into the numerical behavior of F-B and D-B frame models for response and response sensitivity analysis

The results presented in Section 4 shed some light on the different performance of F-B and D-B frame elements. In quasi-static analysis, F-B frame element models achieve the best compromise between accuracy and computational effort by using a single finite element for each physical structural component (beam and/or column). According to the authors experience, the use of five G–L integration points along the element

usually provides more than satisfactory results for response (global and local) quantities. In fact, the Gauss–Lobatto integration rule interpolates exactly a polynomial of order $p = 2n - 3$, where $n$ denotes the number of integration points. Setting $n = 5$ implies the exact integration of a polynomial of order $p = 7$, generally able to accurately describe the effects of material non-linearities on the displacement fields experienced by a single structural component. A higher number of integration points may yield only negligible improvements in the accuracy of the numerical integration, but allows to better capture the continuous nature of the actual inelastic behavior of structural components. In the context of sensitivity analysis, a better description of the continuous inelastic behavior can be crucial to obtain accurate results. In particular, if the material constitutive laws are not continuously differentiable (as in the case of the $J_2$ plasticity model used herein), the use of a higher number of integration points captures better the spreading of the inelastic behavior along the structural member, with two main consequences: (a) the number of spurious discontinuities (generated by spatial discretization of material behavior) increases, and (b) the magnitude of these discontinuities decreases (see Figs. 8(a) and 19(a)). The actual discontinuities (inherent to the physical problem) are not affected by varying the number of integration points as shown in Figs. 11(a) and 22(a). D-B frame element models also exhibit smearing of the spurious discontinuities with increasing number of integration points (see Figs. 7(b), 8(b), 10(b) and Figs. 18(b), 19(b), 21(b)). However, increasing the number of integration points alone is not sufficient to reduce the error inherent to the D-B formulation, which is due to the approximation of the axial and flexural displacement fields with a linear and a third order polynomial, respectively. In particular, when spurious discontinuities generate an oscillatory behavior in response sensitivities, the amplitude of the oscillations can be reduced simply by increasing the number of integration points along each element. However, the average trend of the calculated response sensitivities can be corrected (toward the exact solution) only by refining the mesh, i.e., increasing the number of elements and thus the number of degrees of freedom in the model, as shown in Fig. 39 for the cantilever beam model used as first application example in this paper (see Section 4.1).

The above observations are mainly based on quasi-static analysis studies, but they can be extended to dynamic analysis cases, provided that other important aspects are taken into account. In particular, it is worth noting that: (a) the discontinuities in response sensitivities are more difficult to detect in dynamic analysis than in quasi-static analysis; (b) the accurate and consistent modeling of inertia and damping properties is as important as the accurate prediction of stiffness and restoring force properties, for which the F-B formulation has been proved superior to the D-B one; and (c) accuracy in response sensitivities is more demanding in terms of mesh refinement than the same level of accuracy in the corresponding response quantities. Typically, a mesh in which each structural member is modeled by a single F-B frame element

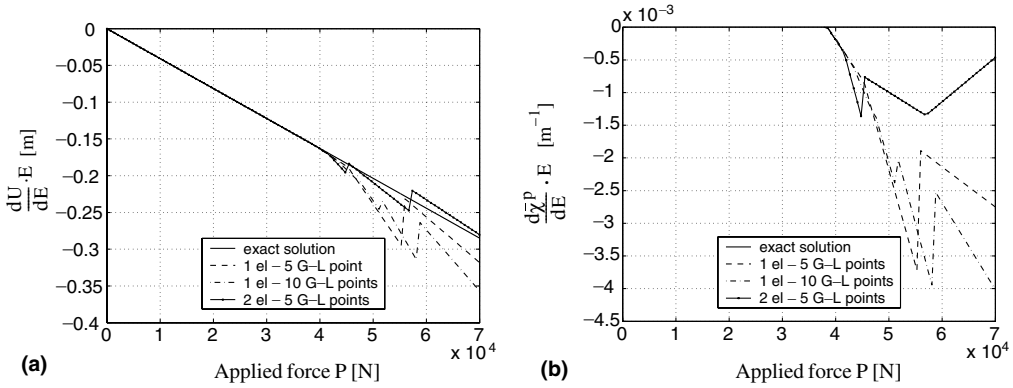


Fig. 39. Spurious discontinuities in the D-B models of the cantilever beam: (a) vertical tip displacement sensitivity to Young's modulus $E$ and (b) sensitivity of the cumulative plastic curvature at the fixed end to Young's modulus $E$.

with five G–L points yields accurate results for response quantities in the context of a dynamic structural analysis. However, unlike in the quasi-static case, increasing the number of integration points per element may not be sufficient for improving the accuracy of response sensitivities to a required level, and refining the mesh may be necessary. This result is not due to an inherent limitation of F-B elements, which generally perform better than D-B elements, but it has to be seen as a direct consequence of the increased difficulty of the response sensitivity problem when compared to the response problem.

## 6. Conclusions

This paper presents an accurate and insightful comparison of the procedures for computing response sensitivities to material and discrete loading parameters for displacement-based and force-based materially-non-linear-only finite element models of structural frame systems. Both procedures emanate from the direct differentiation method, and consist of differentiating exactly the incremental-iterative numerical scheme for the finite element response calculation. Comparison of their implementation in a general-purpose non-linear finite element analysis program based on the direct stiffness method is discussed in great detail.

Three representative application examples are provided: a cantilever steel beam and a simple statically indeterminate frame both subjected to a non-linear quasi-static pushover analysis, and a five-storey, one-bay steel moment-resisting frame subjected to a non-linear dynamic analysis for earthquake base excitation. Closed-form solutions for the response and response sensitivities are available for the first two examples. The non-linear inelastic material model used in the examples consists of the 1-D $J_2$ plasticity model, which describes the moment–curvature constitutive law at the section level. However, the differentiation methods compared in this paper apply to any material constitutive model that can be formulated analytically.

Based on the results presented, it is concluded that the established superiority of force-based (F-B) over displacement-based (D-B) frame elements in terms of trade-off between accuracy in response computations and computational effort is even emphasized for response sensitivity analysis. While for D-B frame element models a significant refinement of the finite element mesh is necessary in order to obtain accurate response sensitivity results, in the case of F-B frame element models, the mesh used for accurate response computation also provides satisfactory response sensitivity results.

The superiority of F-B over D-B elements established in this paper for finite element response sensitivity analysis could have significant impact on any kind of applications that requires response sensitivity analysis. Such applications include structural reliability analysis, structural optimization, structural identification, and finite element model updating.

## Acknowledgement

Partial supports of this research by the National Science Foundation under Grant No. CMS-0010112 and by the Pacific Earthquake Engineering Research (PEER) Center through the Earthquake Engineering Research Centers Program of the National Science Foundation under Award No. EEC-9701568 are gratefully acknowledged. The authors are also thankful to the anonymous reviewers for their constructive criticism of the paper.

## References

[1] J.S. Arora, J.B. Cardoso, A design sensitivity analysis principle and its implementation into ADINA, Comput. Struct. 32 (1989) 691–705.

[2] K.K. Choi, J.L.T. Santos, Design sensitivity analysis of nonlinear structural systems, Part I: theory, Int. J. Numer. Methods Engrg. 24 (1987) 2039–2055.
[3] A.K. Chopra, Dynamics of Structures: Theory and Applications to Earthquake Engineering, Second ed., Prentice-Hall, Englewood Cliffs, NJ, 2001.
[4] J.P. Conte, Finite element response sensitivity analysis in earthquake engineering, in: Earthquake Engineering Frontiers in the New Millennium, Spencer & Hu, Swets & Zeitlinger, 2001, pp. 395–401.
[5] J.P. Conte, M. Barbato, E. Spacone, Finite element response sensitivity analysis using force-based frame models, Int. J. Numer. Methods Engrg. 59 (2004) 1781–1820.
[6] J.P. Conte, P.K. Vijalapura, M. Meghella, Consistent finite-element response sensitivity analysis, J. Engrg. Mech. (ASCE) 129 (2003) 1380–1393.
[7] O. Ditlevsen, H.O. Madsen, Structural Reliability Methods, Wiley, New York, 1996.
[8] F.C. Filippou, FEDEASLab: a Matlab toolbox for linear and nonlinear structural analysis, Private communication, 2002.
[9] P. Franchin, Reliability of uncertain inelastic structures under earthquake excitation, J. Engrg. Mech. (ASCE) 130 (2004) 180–191.
[10] M. Kleiber, H. Antunez, T.D. Hien, P. Kowalczyk, Parameter Sensitivity in Nonlinear Mechanics: Theory and Finite Element Computations, Wiley, New York, 1997.
[11] Matlab, High performance numeric computation and visualization software, User's Guide, The MathWorks Inc., Natick, MA, 1997.
[12] A. Neuenhofer, F.C. Filippou, Evaluation of nonlinear frame finite-element models, J. Struct. Engrg. (ASCE) 123 (1997) 958–966.
[13] E. Spacone, V. Ciampi, F.C. Filippou, Mixed formulation of nonlinear beam finite element, Comput. Struct. 58 (1996) 71–83.
[14] E. Spacone, F.C. Filippou, F.F. Taucer, Fibre beam-column element for nonlinear analysis of R/C frames, Part I: formulation, Earthquake Engrg. Struct. Dyn. 25 (1996) 711–725.
[15] E. Spacone, F.C. Filippou, F.F. Taucer, Fibre beam-column element for nonlinear analysis of R/C frames, Part II: application, Earthquake Engrg. Struct. Dyn. 25 (1996) 727–742.
[16] J.J. Tsay, J.S. Arora, Nonlinear structural design sensitivity analysis for path dependent problems, Part I: general theory, Comput. Methods Appl. Mech. Engrg. 81 (1990) 183–208.
[17] J.J. Tsay, J.B. Cardoso, J.S. Arora, Nonlinear structural design sensitivity analysis for path dependent problems, Part II: analytical examples, Comput. Methods Appl. Mech. Engrg. 81 (1990) 209–228.
[18] Y. Zhang, A. Der Kiureghian, Dynamic response sensitivity of inelastic structures, Comput. Methods Appl. Mech. Engrg. 108 (1993) 23–36.